Accepted Manuscript

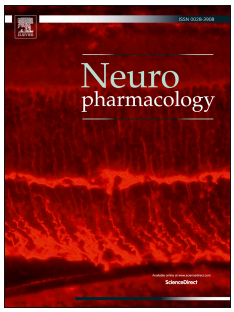

A challenge finding P2X1 and P2X4 ligands

Paul Beswick, Ben Wahab, Mark A. Honey, Michael Paradowski, Ke Jiang, Martin Lochner, Ruth D. Murrell-Lagnado, Andrew J. Thompson

PII: S0028-3908(19)30234-5

DOI: https://doi.org/10.1016/j.neuropharm.2019.107674

Article Number: 107674

Reference: NP 107674

To appear in: *Neuropharmacology*

Received Date: 12 March 2019

Revised Date: 24 May 2019

Accepted Date: 17 June 2019

Please cite this article as: Beswick, P., Wahab, B., Honey, M.A., Paradowski, M., Jiang, K., Lochner, M., Murrell-Lagnado, R.D., Thompson, A.J., A challenge finding P2X1 and P2X4 ligands, *Neuropharmacology* (2019), doi: https://doi.org/10.1016/j.neuropharm.2019.107674.

A challenge finding P2X1 and P2X4 ligands

Paul Beswick[£], Ben Wahab[£], Mark A. Honey[£], Michael Paradowski[£], Ke Jiang[$], Martin Lochner[$], Ruth D. Murrell-Lagnado[£], Andrew J. Thompson[*]

[£]Sussex Drug Discovery Centre, School of Life Sciences, University of Sussex, Brighton, UK

[*]Department of Pharmacology, University of Cambridge, Cambridge, UK

[$]Institute of Biochemistry and Molecular Medicine, University of Bern, Bühlstrasse 28, 3012 Bern, Switzerland

Key Words: antagonist, agonist, P2X1, P2X4, ligand, screen, ion channel, function, two-electrode voltage clamp, microplate

Abbreviation: structure-activity relationship, SAR; adenosine tri-phosphate, ATP

ABSTRACT

Identifying novel small-molecule P2X1 and P2X4 ligands with sub-type specificity and high-affinity remains a pharmacological challenge. Here we use computational methods, electrophysiology and fluorescent microplate assays to screen for ligand candidates acting at these receptors. Modelling and docking identified 80 compounds for testing at P2X4 receptors, and 20 of these showed > 50% inhibition in fluorescence-based assays, making them appealing for further SAR studies. Confirmation of activity by two-electrode voltage clamp, followed by their elaboration resulted in only minor improvements in potency, with the highest IC_{50} being 295 µM. Testing on P2X1 receptors, resulted in a series of biguanide compounds that yielded a maximum IC_{50} of 100 µM, but no consistent SAR could be found. Potencies of established antagonists gave expected results, although the measured potencies varied between techniques and no antagonism could be found for compounds such as paroxetine, carbamazepine, 9(10*H*)-acridanone, acridinol and phenoxazine-type heterocycles. This study highlights the challenge of identifying P2X4 and P2X1 ligands and suggests that a combination of complimentary approaches is needed if we are to be confident of ligand activities at these receptors.

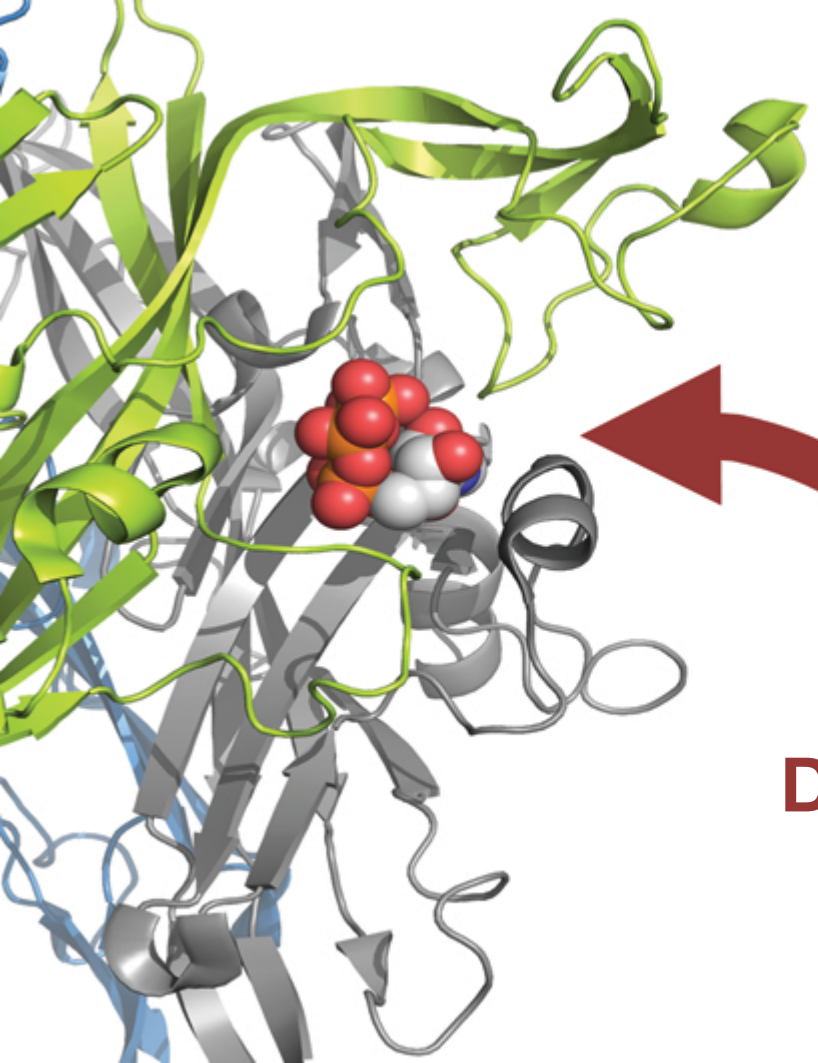

P2X4
P2X1

DOCKING
TEVC
FMA

INTRODUCTION

There are seven P2X receptor subunits that can assemble into a range of functional homomeric and heteromeric receptors. All are trimeric, transmembrane ligand-gated ion channels, the activation of which opens a central ion-conducting pore and results in a wide range of biological functions.

For P2X1 and P2X4 receptors there is still a clear clinical need for selective ligands that has not been met. For example, the development of P2X1 receptor-selective ligands could lead to the development of safe and effective treatments for the prevention of blood clotting, or in combination with β–adrenergic antagonists, as non-hormonal male contraceptives (White et al., 2013). In transgenic mice P2X1 knockout blocks sympathetically mediated sperm transport through the vas deferens and also causes a resistance to systemic thromboembolism. In contrast, overexpression causes the mice to exhibit platelet hyperreactivity and thrombosis at high shear (Hechler et al., 2003; Oury et al., 2003). For P2X4 receptors, a knockout mouse model revealed an association between P2X4 and neuropathic pain, inflammatory-associated pain and tactile allodynia (Tsuda, Kuboyama, Inoue, Nagata, Tozaki-Saitoh & Inoue, 2009; Tsuda, Masuda, Tozaki-Saitoh & Inoue, 2013). Furthermore, P2X4 receptors are upregulated in neuronal injury or inflammation (Tsuda, Masuda, Tozaki-Saitoh & Inoue, 2013). As neuropathic pain is often resistant to currently available analgesics, inhibition of P2X4 receptors could therefore represent a new therapeutic target for its management (Jurga, Piotrowska, Makuch, Przewlocka & Mika, 2017). Increased P2X4 receptor activity has been shown to be cardioprotective and to promote remyelination in a mouse model of multiple sclerosis (Ralevic, 2015; Zabala et al., 2018). These findings suggest that positive allosteric modulators of P2X4 will also have therapeutic potential.

ATP is the native agonist of all P2X receptors and there are α,β- and β,γ-meATP derivatives that have similar actions, revealing the importance of the phosphate side-chain in agonist recognition. Several weak, nucleotide and non-nucleotide antagonists have also been discovered, but many of these are not selective for P2X receptor subtypes. For example, BzATP activates P2X1, P2X4 and other subtypes, but is also an antagonist of P2Y12 (Bianchi et al., 1999; Ding, Kim, Dorsam, Jin & Kunapuli, 2003). The large polysulfonated compound suramin also inhibits both P2X and P2Y receptors, as well as other G-proteins and proteases such as HIV reverse transcriptase and protein kinase C (Freissmuth et al., 1996; Hensey, Boscoboinik & Azzi, 1989; Jentsch, Hunsmann, Hartmann & Nickel, 1987). Suramin has also acted as a lead structure for the development of additional P2X receptor inhibitors, including derivatives with nanomolar potency, such as NF-449 acting at P2X1 receptors

(North & Jarvis, 2013). Other large, but low affinity antagonists such as PPADS have also acted as leads structures, but these derivatives similarly antagonise several subtypes, including P2X1 and P2X4, among others (Syed & Kennedy, 2012).

Since antidepressants were found to be effective against neuropathic pain, a number of the compounds have been tested for inhibitory potency at the P2X4 receptor, with Paraxetine being identified as an allosteric modulator (fig 1). A similar allosteric mechanism has been proposed for 5-BDBD, although a competitive mechanism has also been suggested (Balazs, Danko, Kovacs, Koles, Hediger & Zsembery, 2013; Muller, 2015). The heterocyclic compound phenoxazine was once used as a fabric dye, and its structure has acted as a lead for P2X4 antagonists and a library of *N*-substituted derivatives. The structure of the most active compounds, PSB-12054 (fig 1) and PSB-12062, inhibited P2X4 receptors with nanomolar potency, but also showed activity at other P2X receptor subtypes (Hernandez-Olmos, Abdelrahman, El-Tayeb, Freudendahl, Weinhausen & Muller, 2012). The heterocyclic anticonvulsant carbamazepine and its derivatives are also reported as potent P2X4 receptor antagonists and the most potent in this series (*N*,*N*-diisopropylcarbamazepine) is also reported to have allosteric behaviour. More recently, BX430 was discovered, and was again described as an allosteric modulator that lacks subtype specificity. However, unlike many of the previous reports, a range of methods was used to validate its mechanism of action, including patch clamp and calcium imaging (Ase, Honson, Zaghdane, Pfeifer & Seguela, 2015).

The relatively small number of commercially available, small, potent, P2X1 and P2X4 subtype-selective ligands highlights the challenge of targeting these receptors. In recent years attempts to identify new P2X1 and P2X4 ligands has seen some successes. Here we describe our efforts to screen for P2X1 and P2X4 ligands and report on the challenges we faced. For the majority of hits identified using a fluorescence-based approach, we were unable to measure consistent responses in subsequent electrophysiological assays. Furthermore, although some well-established inhibitors were active in both assays, for several more recently disclosed compounds, neither of our assays was able to reproduce the inhibition that was previously reported. We therefore conclude that screening programs should include a range of methods to validate hits.

METHODS

Computational modelling: A human homology model was created from the co-crystal structure of ATP with zebrafish P2X4 (4DW1; Hattori & Goaux, Nature 485 207-212. 2012) and was assessed (B-factors, Ramachandran compliance). The homology model was built within MOE 2015.10, using the canonical human P2XA sequence Q99571. The direction of side-chains of variant residues within 5 Å of ATP (G142, R142 and A292) was maintained by holding the backbone atoms in the same positions and the model subsequently relaxed by minimisation. The model was checked for consistency using Ramachandran analysis and had 96.27% of resides in favoured positions, a MolProbity Score of 1.87, and an alignment of 0.316Å RSMD versus the 4DW1 structure.

The water map from 4DW1 was transferred and the system was relaxed. Pocket waters were analysed, and those which bridged ATP interactions were retained, and those that did not were removed. B-Factor analysis showed these to be no less labile than the average for the structure.

The virtual screening cascade was built of the following steps: 1) assess and prepare suitable 3D structural information, 2) design and screen pharmacophores as a pre-screening step, 3) conduct docking based on pharmacophore outputs, 4) analysis and clustering, 5) medicinal chemistry appraisal and, 5) purchase.

An internal VS library ("SUNdb") was deployed in this VS cascade, containing over 1.8 million compounds from preferred suppliers with a high level of content trust (fig 2). SUNdb is pre-filtered for both PAINS and other undesirable features using internal proprietary filtering systems, with filtration performed in Knime (Knime AG, 8005 Zurich, Switzerland).

Pharmacophore pre-screening was conducted using two Boolean pharmacophores; one based on the ATP interactions (5 features with a minimum of 4 required) and a global pocket pharmacophore (29 features with a minimum of 5 required). Both pharmacophores were conducted with void spacing around the protein. This approach was designed to create two hit sets; one with a similar binding mode to ATP, and a second with a very diverse library of moieties that are predicted to bind with more generally. Given that the binding pocket is significantly open to solvent, the diverse pharmacophore would require significant filtering to ensure that the pharmacophore passes were rational.

The output of the pharmacophore screen was docked into the human P2X4 homology model with conserved waters. For the ATP-mode mimetic materials, docking was conducted by pharmacophore placement. Pharmacophore screening and docking was conducted in MOE 2015.10 using customised flexible docking protocols (MOE, Chemical Computing Group, QC H3A 2R7, Montreal, Canada).

Post-docking analysis and clustering allowed 100 exemplars of docked materials from each pharmacophore mode to be assessed by medicinal chemists, with a total of 80 materials selected for purchase. Due to the nature of the diversity, the clustering was reasonably severe, meaning that there was a high dissimilarity between centroids of the clusters. A result of diversity means that any hit would likely be a singleton, and so each cluster was held aside for follow up purchasing or synthesis.

Compounds: Screening compounds were bought commercially from IOTA Pharmaceuticals (Cambridge, UK), ChemBridge (San Diego, CA, USA), Sigma Aldrich (St Loius, MO, USA) or were synthesised *de novo* according to published procedures (Hernandez-Olmos, Abdelrahman, El-Tayeb, Freudendahl, Weinhausen & Muller, 2012).

Cell Culture & Receptor Expression: Human P2X1 (Accession: P51575) or human P2X4 (Accession: Q99571) subunit cDNA was cloned into pGEMHE for oocyte expression. cRNA was *in vitro* transcribed from linearised plasmid cDNA template using the mMessage mMachine Ultra T7 Transcription kit (Ambion, Austin, Texas, USA). Stage V and VI oocytes were injected with 50 nl of 100-200 ng / µl cRNA (5 - 25 ng injected), and currents were recorded 1 - 4 days post-injection.

Cell lines: Human embryonic kidney (HEK) 293T cells were grown on 90 mm round tissue culture plates as monolayers in DMEM/F12 (Life Technologies) supplemented with 10% foetal bovine serum (FBS; Sigma Aldrich) at 37^{o}C in a moist atmosphere containing 5% CO_2.

A HEK293T cell-line stably expressing hP2X1 receptors was constructed by transducing with pLV-tTR-Krab-Blast to create the HEK293-tTR-Krab-Blast cell line. After selection of transduced cells with Blasticidin, this cell line was transduced with pLV-P2X1-IRES.IFP1.4 to create the inducible hP2X1-FLAG-IRES-IFP1.4 cell line that was clonally selected for high expression (Ruepp, Brozik, de Esch, Farndale, Murrell-Lagnado & Thompson, 2015).

HEK293T cells expressing P2X4 receptors were made by transient transfection of cDNA using polyethyleneimine (PEI: 25 kDa, linear, powder, Polysciences Inc., Eppelheim, Germany). In brief, 30 ml of PEI (1 mg ml^{-1}), 5 mg cDNA and 1 ml DMEM/F12 were incubated for 10 min at room temperature, added drop wise to a 90 mm plate of 70 - 80% confluent HEK293T cells, and incubated for 2 - 3 days before use.

Fluorometric Microplate Assays: Assays were performed using methods similar to those described elsewhere (Thompson, Verheij, Leurs, De Esch & Lummis, 2010). In brief, fragments were assessed for both agonist and antagonist activities using HEK293T cells stably expressing P2X receptors incubated for 45 min with 50 µl of a fluorescent membrane potential (dye FLIPR Membrane Potential Assay Kit, Molecular Devices, Wokingham, UK) dissolved in buffer (mM: 115 NaCl, 1 KCl, 1 $MgCl_2$, 1 $CaCl_2$, 10 HEPES, 10 D-Glucose, pH 7.4). Dye-loaded cells were transferred to a FlexStation III (Molecular Devices) where compound applications were made without removing the dye. At recording intervals of 1.2 s, baseline fluorescence was recorded for 20 s, followed by a further 60 s after the addition of compounds. Ultimately two applications were made to the same cells. In the first of these agonist activity was assessed by adding 50 µl novel fragment (final concentration = 300 µM) to each well. Following the completion of the first application, a second 50 µl application of 30 µM ATP (final concentration = 10 µM) was then added to the same cells. A response upon the first (fragment) application and an absence of a response on the second (ATP) application indicated agonist activity followed by inhibition as a result of receptor desensitisation. In contrast, an antagonist did not elicit a response in the first application and inhibited the subsequent ATP response. The absence of a response during the first application and a robust ATP response upon the second application indicated that the fragment was inactive.

In addition to testing fragments, the reproducibility of each experiment was assessed by including an ATP concentration-response in the first column and a saline control in the last column of the first application. This ensured ATP activation at appropriate concentrations at the start of the experiment and that buffer alone did not alter the baseline fluorescence. The saline control in the first application also meant that an ATP concentration-response could be performed at the end of the second application. This allowed cell viability to be assessed by comparing the ATP concentration-response at the start of the first application with the ATP concentration-response at the end of the second application. At least two replicates were performed and compounds scored as hits when activity was observed on two plates. Following the identification of active compounds from these single-concentration screens, the same procedure was used to subsequently test hits for

concentration-dependence to confirm their activity and to obtain a measure of their potency. Measurements from these concentration-dependence experiments were fitted using Equ 1 below.

Applying novel compounds and a known agonist to the same cells had several advantages, namely that 1) agonist, antagonist and allosteric modulators were identified in a single screen, 2) which reduced material costs, 3) the 16 min time period between the first and second applications allowed fragments to equilibrate in the presence of the cells before the second ATP application was added and, 4) reproducibility was improved because the same cells were subjected to both applications.

Oocyte Maintenance: Oocytes from *Xenopus laevis* were purchased from EcoCyte Bioscience (Castrop-Rauxel, Germany) and stored at 16°C in ND96 (96 mM NaCl, 2 mM KCl, 1 mM $MgCl_2$, 5 mM HEPES, pH 7.5).

Electrophysiology: Using two electrode voltage clamp (TEVC), *Xenopus* oocytes were routinely clamped at -60 mV using an OC-725 amplifier (Warner Instruments, Connecticut, USA), NI USB-6341 X Series DAQ Device (National Instruments, Berkshire, UK) and the Strathclyde Electrophysiology Software Package v4.7.3 (University of Strathclyde, UK). Micro-electrodes were fabricated from borosilicate glass (GC120TF-10, Harvard Apparatus, Edenbridge, Kent, UK) using a two stage horizontal pull (P-1000, Sutter Instrument Company, California, USA) and filled with 3 M KCl. Pipette resistances ranged from 0.8-2.0 MΩ. Oocytes were placed in a perfusion chamber made from 2 mm wide x 30 mm long silicon tubing that was cut in half lengthways (total volume ~ 0.1 ml), and were perfused with ND96 at a rate of 12 ml min^{-1}. Drug application was via a simple gravity fed system calibrated to run at the same rate. For inhibition curves, antagonists were routinely co-applied in the presence of either 0.5 µM ATP (EC_{50} of hP2X1) or 3 µM ATP (EC_{50} of hP2X4), or continuously applied for 1 min before the co-application of these ATP concentrations. A 4 min wash was used between drug applications for hP2X1 and 3 min for P2X4.

Data Analysis: Measurements from the FlexStation III were recorded using the integrated software SoftMax Pro v5.4.5 (Molecular Devices). Analysis of concentration-dependence was performed with GraphPad Prism v5.00 (GraphPad Software, San Diego, CA, USA). Peak fluorescence was measured at a range of ligand concentrations and normalised to the maximum peak fluorescence for the same experiment. The mean and S.E.M. for a series of oocytes was plotted against agonist or antagonist concentration and iteratively fitted to the following equation:

$$y = I_{\min} + \frac{F_{\max} - F_{\min}}{1+10^{\log(R_{50}-x)^{nH}}}$$

(Equ. 1)

where F_{min} is the baseline fluorescence, F_{max} is the peak fluorescence, R_{50} is the concentration of ligand needed to generate a half-maximal response, x is the ligand concentration and n_H is the Hill slope.

For electrophysiological measurements, peak current responses were measured across a range of concentrations and normalised to the maximum peak current for the same oocyte. The mean and S.E.M. for a series of oocytes was plotted against agonist or antagonist concentration and iteratively fitted to the following equation using GraphPad Prism v5.00:

$$y = I_{min} + \frac{I_{max} - I_{min}}{1 + 10^{\log(EC_{50} - x)^{n_H}}} \quad \text{(Equ. 2)}$$

where I_{min} is the baseline current, I_{max} is the peak current evoked by agonist, EC_{50} is the concentration of agonist needed to evoke a half-maximal response, x is the ligand concentration and n_H is the Hill slope.

For single-point assays 300 µM of test compound was co-applied in the presence of ATP and the peak current responses normalised to the peak current response in the presence of ATP alone. Based upon a simple antagonist mechanism of action (n_H = 1), the single point measurement was used to predict the IC_{50} based on the Equ 2.

RESULTS

Computational modelling and ligand docking into hP2X4 receptors initially identified 80 compounds that were available from the IOTA fragment library (fig 3). These fragments formed a diverse group, with scaffolds largely represented by a series of heterocyclic compounds. Single-point FMA screening of these 80 fragments on hP2X4 yielded the data shown in Table 1. For the majority of these compounds, single-point FMA assays were also performed on hP2X1 receptors to probe for receptor selectivity (Table 1).

Of the 80 fragments identified from *in silico* docking into hP2X4, 20 fragments reached the 50% inhibition threshold that was used to progress hits for further study. For these, the ten highest potency compounds were also tested by two-electrode voltage clamp on hP2X4 at a single concentration of 300 µM (Table 2). The results obtained with the TEVC assay were not consistent with the FMA data as only **35**, **57** and **66** consistently inhibited the agonist response in both assays, and the remaining seven compounds produced no inhibition of the P2X4 mediated current. Two of these seven compounds (**38** and **64**) produced a significant potentiation of the TEVC response despite indicating inhibition using FMA. For the three compounds that consistently inhibited hP2X4 receptors at 300 µM, IC_{50} values were determined by measuring concentration-dependent inhibition by TEVC (figs 4A – 4D). To test for non-specific effects we also tested these fragments on uninjected oocytes at 300 µM. Compounds **38**, **57** and **66** had no effect, while 300 µM **35** caused a hyperpolarising current that indicated off-target effects (fig 4E). This could be mistaken for hP2X4 inhibition as it would reduce the amplitude of the ATP-evoked current (fig 4F). It is noteworthy that **35** contains a number of structural elements that can cause assay interference, namely nitro-phenyl and dicyanobenzyl groups, and this could be the case here. Hence this fragment was not considered as a genuine hit for further investigation. Single-point TEVC measurements of the same ten fragments on hP2X1 revealed only minor differences in compound activities when compared to hP2X4, with the only difference being **34** which displayed almost complete inhibition of hP2X1 and only limited effects on hP2X4.

To evaluate the potential of the initial hit fragments to become leads for future hP2X4 drug discovery, six compound series were identified for further evaluation based on (a) encouraging activity in both the FMA and TEVC assays or, (b) activity in the FMA assay and structural similarity to reported hP2X4 ligands. The primary objective of the exercise was to establish if robust structure-activity relationships (SAR) could be established and positions within the molecule identified that

would allow future elaboration to increase potency and selectivity. Additional considerations regarding physicochemical properties were also important in the choice of compounds for testing, and molecules with high lipophilicity, high polarity, large aromatic ring count and known structural alerts were avoided. For this initial exercise, commercially available compounds were selected with either a high degree of similarity to the initial hit fragments to eliminate false positives and singletons, or with the scaffold substituted at key sites to probe for additional binding site regions that could increase potency. Given the absence of structural information at the time the work was performed, robust pharmacophore analogues with as many diverse single substitutions were selected. In certain cases no suitable analogues were commercially available and key molecules were synthesised to complement the sets.

First priority was given to those compounds that showed promising activity in both FMA and TEVC screening formats. From this, three groups were considered worthy of further consideration. These included a series of amines represented by **20**, **21** and **22**, a series of diarylmethanes represented by **30** and **66**, and a series of diaryl heterocycles represented by **32** and **34**.

Second priority was given to fragments that shared structural similarity to previously reported hP2X4 ligands but only showed activity with FMA. Two additional groups were selected in this category, including a series of indole-derived molecules based on the tetracyclic hit **10** and the structurally related hits **7**, **9**, **12**, **13** and **16**. As well as being a cluster of related hits, these molecules shared some features with carbamazepine (fig 1). A series of carbamates and ureas represented by **41**, **48** and **64**, were structurally similar to the P2X4 modulator BX 430 (fig 1), and were also selected.

Despite the encouraging activity observed with **20**, **21** and **22**, TEVC testing of close analogues failed to identify compounds with encouraging activity profiles (Table 3A). Indeed, the majority of analogues tested were inactive. To be confident of the results, the original fragments (**1** - **80**) were analysed and found to be of a high degree of purity. In addition, freshly synthesised material prepared in our laboratory demonstrated a similar level of activity when tested, confirming the original observations. To further investigate the structural basis for the loss of activity in the close analogues, a series of new compounds were chosen with close structural similarity to the original hit fragments. This resulted in a further set of compounds in which the second ring of the bicyclic core was removed (Table 3B). However, this series also failed to identify any compounds with sufficient activity for further progression. A series of analogues inspired by **30**, **32** and **66** also had no activity (Table 3C) as did structural analogues of **41**, **48** and **64** (Table 3D).

Fragment **10** initially produced an encouraging response when tested with FMA, and given the structural similarity to compounds such as carbamazepine, represented an attractive start point for further evaluation. From a medicinal chemistry perspective, the tetracyclic nature of the molecule was not attractive and consideration was given to removing this element in analogues selected for screening. It was also proposed that analogues should replace the indole with benzimidazole as the incorporation of the additional nitrogen atom would potentially increase solubility and additionally offer a further H-bond acceptor. At total of 39 structurally related analogues were selected for testing (Table 3E). The first of these, **146**, showed encouraging activity in FMA assays, as did the analogues **149** and **169** in which aromatic groups were appended to the amino group. Unfortunately, a more expanded SAR failed to identify further improvements and when tested in TEVC assays none of these compounds demonstrated activity, indicating that they were false positives.

Following this failure to identify robust hits it was decided to test representatives of structural chemotypes not represented within the library. We consequently tested a range of 15 biguanide compounds and derivatives that were remaining from previous screening campaigns. We measured activities by concentration-response using TEVC on hP2X1 and found encouraging results from our initial screens (Table 4). Compounds with activity showed highly reproducible inhibition, with the lowest IC_{50} value being 100 µM for **216** (fig 5). However, no further improvements in inhibitory activity or consistent SAR could be seen in the series and no other compounds were explored.

The lack of activity that we observed with these different series of compounds also prompted us to investigate the potency of ligands that were previously reported to inhibit the hP2X4 receptor. One such ligand, that was previously reported by Nippon Chemiphar to be a micromolar antagonist of hP2X4, was synthesised and given the name UoS14919 (fig 1) (Ushioda, Kobayashi, Saito, Sakuma, Imai & Inoue). UoS14919 was first tested using FMA and inhibited the hP2X4 agonist response with an IC_{50} of 61 nM (fig 6A). In TEVC, co-application of ATP with 10 µM UoS14919 did not inhibit hP2X1 (I_{max} = 0.96 ± 0.04, n =3), but caused 50% inhibition of hP2X4 (I_{max} = 0.50 ± 0.13, n = 3). A 30 s pre-application of UoS14919 further increased potency at hP2X4, as shown by the total and reversible inhibition at the same 10 µM concentration (fig 6B). Because of the high affinity of this compound it was not possible to make equilibrium measurements using TEVC and no concentration-response measurements were undertaken using this technique.

Two further compounds have been reported by Hernandez-Olmos *et al*. (Hernandez-Olmos, Abdelrahman, El-Tayeb, Freudendahl, Weinhausen & Muller, 2012). These are phenoxazine (PSB-12054; IC_{50}; hP2X4 = 0.19 μM; hP2X1 = 6.52 μM) and acridinol (IC_{50}; hP2X4 =2.44 μM, hP2X1 = 0.60 μM) (fig 1). Limited solubility dictated that these compounds could be maximally applied at concentrations of 75 μM and 93 μM respectively, concentrations that should result in complete inhibition. However, neither of these compounds showed any appreciable inhibition using either FMA or TEVC when either co-applied or pre-applied for 1 min (fig 6C). Other reported hP2X4 antagonists such as carbamazepine, paroxetine, and 9(10*H*)-acridanone similarly did not show agonist or antagonist activities in our FMA and TEVC assays (fig 1). In contrast, the established ligands NF449 and suramin both caused inhibition (data not shown).

DISCUSSION

Here we report the use of fragment-based drug discovery to screen for ligands acting at hP2X4 receptors. This resulted in low potency hits that were confirmed by TEVC to have a maximum IC_{50} of 295 μM. Further elaboration of these lead compounds did not result in the anticipated increases in activity that we have previously seen at other receptors (Thompson, Verheij, Leurs, De Esch & Lummis, 2010; Thompson, Verheij, van Muijlwijk-Koezen, Lummis, Leurs & de Esch, 2013; Verheij, Thompson, van Muijlwijk-Koezen, Lummis, Leurs & de Esch, 2012). There were also inconsistencies in the results obtained using FMA with voltage-sensitive dyes and electrophysiological recordings using TEVC, the latter of which is the gold-standard for measuring the effects of compounds on ion channels. Using TEVC we were also able to show inhibition by several well-established antagonists, but were unable to reproduce the antagonism reported for compounds that have been identified more recently using calcium-based fluorescent assays (Hernandez-Olmos, Abdelrahman, El-Tayeb, Freudendahl, Weinhausen & Muller, 2012).

Our most potent hit structures are very different from classic P2X ligands, such as nucleotide analogues BzATP, non-hydrolysable ATP derivatives, sulfonated dye compounds (suramin, NF-449) and pyridoxal phosphate congeners (PPADS). All of these compounds are non-selective and often highly charged, and therefore difficult to develop into pharmacologically useful compounds. Instead, our hit structures are small and more drug-like heterocyclic compounds that could represent more reasonable starting points for further synthetic optimisation. However, in our current study, an extensive investigation of potential SAR failed to identify any robust series. Such a finding is disappointing as there are several promising structures within the sets. For example, those in tables

3D and 3E contain an indole or benzimidazole core in some instances fused to a six membered ring, templates that are common in pharmacologically active molecules that are well characterised and with proven mechanisms of action. This is an attractive feature that was the key driver in the selection of this structure for further work, while the precedence of similar active molecules in the literature indicates that any identified hits would not be false-positives resulting from assay interference. A lack of SAR therefore suggests the influence of biological phenomena such as the original hits already being optimally bound to a low affinity site or non-spcecifc interactions that are not reproduced in the analogues. Other reasons could include the precence of trace impurities that were present in the original hits, but we believe that this is unlikley as hit compounds were thoroughly analysed upon receipt and several were resynthesied and retested. Other examples of promising structures included compounds such as **30**, **32** and **66**, which all contain a diarylmethane group that is common amongst inhibitors of various ion channels (e.g. flunarizine, diphenhydramine and chlorphenoxamine). However, these hits also turned out to be poor starting points for elaboration (Table 3C), which could be due to the possibility of diarylmethane -containing molecules having a precedence of forming aggregates in solution, leading to changes in their absorption properties (Attwood, 1976). For compounds such as **41**, **48** and **64** poor solubility might also be an explanation, although no obvious precipitate was seen during our experiments.

A number of hits from the IOTA fragment library also demonstrated activity when screened against hP2X1, namely **20**, **35**, **38**, **64** and **66**. Similar to the search for hP2X4 ligands, these hits did not produce any convincing SAR, and as they do not contain any structural elements known to produce assay-interference, it is possible that they have non-specific effects. Following this failure to identify robust hits, representatives of structural chemotypes not represented within the library were also tested on hP2X1. Initial results were encouraging for a series of biguanides where robust and reproducible inhibition was seen using TEVC, and consequently it was possible to measure IC_{50} values for several of these compounds (Table 4). Indeed, such compounds also show activity at other ligand-gated ion channels (Lochner & Thompson, 2014). However, despite obtaining consistent results these compounds did not show consistent SAR that could be used for further elaboration. Again it is difficult to explain why hits could not be converted into a robust series, although one possibility is that biguanides are well documented to bind metal ions and their strongly interaction with calcium may cause a variety of cellular effects (Logie et al., 2012).

Our study struggled to identify consistent SAR. Furthermore, the complex pharmacology and chemical nature of reported P2X4 and P2X1 ligands does not align with currently accepted ‘drug like’

chemical space. In contrast to other members of the P2X receptor family, there is also a paucity of high quality drug like compounds reported to modulate P2X1 or P2X4 activity. For P2X4 these are generally of poor quality, while the only molecules reported to have any interaction with P2X1 are high molecular weight and promiscuous agents such as suramin. These P2X1-active compounds also typically have high lipophilicity that frequently leads to a poor solubility, and is often highlighted as a challenge in medicinal chemistry reviews (Gum, Wakefield & Jarvis, 2012; Jacobson & Muller, 2016). Also, whilst it is not disclosed, their physical chemistry suggests that it is highly likely that these existing P2X-active compounds have poor pharmacokinetic profiles. For example, Nippon Chemiphar have been pioneers in this area and have identified structures such as UoS14919 and NP-1815_PX (fig 1)(Ushioda, Kobayashi, Saito, Sakuma, Imai & Inoue). In the publication describing these structures they highlight the poor solubility of UoS14919, and report that despite having slightly improved solubility, NP-1815_PX is not suitable for oral administration and that intra thecal-dosing has to be employed for *in vivo* testing (Matsumura et al., 2016). As a result, only two molecules are reported to have entered development despite many years of work. This includes NC600 which is described by Nippon Chemiphar as having entered phase 1 studies in June 2016 (communication on company website), and more recently by Bayer who announced they had entered the clinic with an unspecified P2X4 antagonist (communication on company website). It is noteworthy that only Nippon Chemiphar has reported the progression of a molecule past the stage of the preliminary tests that would be applied during the discovery phase of a project, and their molecules do appear to have an encouraging profile despite the poor physicochemical properties. The lack of progression of any other reported compounds suggests unreported challenges. The results we report here are consistent with these difficulties, and highlight the importance of validating hit compounds using a range of pharmacological methods.

In our hands, established P2X ligands such as suramin and NF-449 caused inhibition of both FMA and TEVC responses at expected concentrations, as did UoS14919 (Ushioda, Kobayashi, Saito, Sakuma, Imai & Inoue). In contrast, we were unable to observe pharmacological activities with phenoxazine or acridinol, compounds that have been reported as active following screening of phenoxazine and acridone derivatives using fluorescence-based calcium measurements (Hernandez-Olmos, Abdelrahman, El-Tayeb, Freudendahl, Weinhausen & Muller, 2012). This finding highlights the challenges of identifying P2X ligands and suggests that different methods may yield conflicting results. The lack of activity in our FMA and TEVC assays suggests these compounds may have been false-positives in the calcium-based fluorescence assays (Hernandez-Olmos, Abdelrahman, El-Tayeb, Freudendahl, Weinhausen & Muller, 2012). One possible reason for this could be that the

compounds identified by calcium-based fluorescence were pre-applied. However, even when we used pre-incubation in our assays no inhibition was seen, showing that this is not the case. It is also possible that the calcium-based fluorescence assays reported effects on responses mediated by other cell-surface receptors, or by mobilisation of intracellular stores. Indeed, using our voltage-sensitive dye, we noted that **35** caused a depolarisation that was later identified as a non-specific effect with TEVC. For both carbamazepine and paroxetine there is already literature evidence that demonstrates they may result in calcium entry into various cell types (Pan, Kuo, Shieh, Chen, Kuo & Jan, 2010; von Borstel Smith, Crofoot, Rodriguez-Proteau & Filtz, 2007). The structural similarity of the 9(10*H*)-acridanone and phenoxazine based inhibitors to carbamazepine suggests that they could also affect calcium entry. Compounds such as carbamazepine, 9(10*H*)-acridanone and phenoxazine also all share aromatic structures that will demonstrate absorbance and could interfere with fluorescence-based measurements.

For other ligand-gated ion channels a combination of functional assays and ligand binding has been used to corroborate ligand actions. Examples can include two or more approaches such as electrophysiology, radioligand binding, surface plasmon resonance and flow cytometry, or by confirming the binding of ligands by mutagenesis of the target receptor (Lochner & Thompson, 2015). To date there are few reports of P2X4 or P2X1 ligands that have been assessed by multiple methods. An exception is the study by (Hernandez-Olmos, Abdelrahman, El-Tayeb, Freudendahl, Weinhausen & Muller, 2012) which revealed activity in calcium-based fluorescence assays and followed these up with radioligand competition assays. However, as no competition was observed with radiolabelled ATP it was concluded that the ligands were non-competitive at the orthosteric site, rather than non-specific. In contrast, where complementary assays have instead given consistent results across differing assay formats, the actions of the resultant ligands have been reproducible (Ase, Honson, Zaghdane, Pfeifer & Seguela, 2015). Both our own studies and this published evidence suggest that verification of potential hits by complimentary methods is needed to provide supporting evidence of their effects and that methods should be sought that yield confirmation of ligand activities.

The results presented here describe the identification of low affinity ligands acting at hP2X4 and hP2X1 receptors. The activities that we measured were too low to be of any pharmacological value, but their structures might provide starting points for further elaboration or as substructures in much larger ligands. Our results also highlight the challenges of achieving consistent results across different assay formats. Such findings appear relatively common within the P2X field. Ideally, all

future studies would therefore include a range of methods to validate hits. This might include a means of identifying the binding site for compounds and competition-based reporter assays to increase confidence in the results.

ACKNOWLEDGMENTS

The British Heart Foundation supported AJT (grant; PG/13/39/30293). RML was supported by EU COST Action BM1046. Thanks are also due to Professor John Atack and Dr Simon Ward for constructive discussions and support.

AUTHORSHIP CONTRIBUTIONS

Participated in research design: AJT, PB, MH, MP, RML, BW

Conducted experiments: AJT

Contributed reagents or analytical tools: KJ, ML, PB

Performed data analysis: AJT, ML, MP

Wrote or contributed to the writing of the manuscript: AJT, PB, BW, RML

REFERENCES

Ase AR, Honson NS, Zaghdane H, Pfeifer TA, & Seguela P (2015). Identification and characterization of a selective allosteric antagonist of human P2X4 receptor channels. Mol Pharmacol 87**:** 606-616.

Attwood D (1976). Aggregation of antiacetylcholine drugs in aqueous solution: micellar properties of some diphenylmethane derivatives. J Pharm Pharmacol 28**:** 407-409.

Balazs B, Danko T, Kovacs G, Koles L, Hediger MA, & Zsembery A (2013). Investigation of the inhibitory effects of the benzodiazepine derivative, 5-BDBD on P2X4 purinergic receptors by two complementary methods. Cell Physiol Biochem 32**:** 11-24.

Bianchi BR, Lynch KJ, Touma E, Niforatos W, Burgard EC, Alexander KM*, et al.* (1999). Pharmacological characterization of recombinant human and rat P2X receptor subtypes. Eur J Pharmacol 376**:** 127-138.

Ding Z, Kim S, Dorsam RT, Jin J, & Kunapuli SP (2003). Inactivation of the human P2Y12 receptor by thiol reagents requires interaction with both extracellular cysteine residues, Cys17 and Cys270. Blood 101**:** 3908-3914.

Freissmuth M, Boehm S, Beindl W, Nickel P, Ijzerman AP, Hohenegger M*, et al.* (1996). Suramin analogues as subtype-selective G protein inhibitors. Mol Pharmacol 49**:** 602-611.

Gum RJ, Wakefield B, & Jarvis MF (2012). P2X receptor antagonists for pain management: examination of binding and physicochemical properties. Purinergic Signal 8**:** 41-56.

Hechler B, Lenain N, Marchese P, Vial C, Heim V, Freund M*, et al.* (2003). A role of the fast ATP-gated P2X1 cation channel in thrombosis of small arteries in vivo. J Exp Med 198**:** 661-667.

Hensey CE, Boscoboinik D, & Azzi A (1989). Suramin, an anti-cancer drug, inhibits protein kinase C and induces differentiation in neuroblastoma cell clone NB2A. FEBS Lett 258**:** 156-158.

Hernandez-Olmos V, Abdelrahman A, El-Tayeb A, Freudendahl D, Weinhausen S, & Muller CE (2012). N-substituted phenoxazine and acridone derivatives: structure-activity relationships of potent P2X4 receptor antagonists. J Med Chem 55**:** 9576-9588.

Jacobson KA, & Muller CE (2016). Medicinal chemistry of adenosine, P2Y and P2X receptors. Neuropharmacology 104**:** 31-49.

Jentsch KD, Hunsmann G, Hartmann H, & Nickel P (1987). Inhibition of human immunodeficiency virus type I reverse transcriptase by suramin-related compounds. J Gen Virol 68**:** 2183-2192.

Jurga AM, Piotrowska A, Makuch W, Przewlocka B, & Mika J (2017). Blockade of P2X4 Receptors Inhibits Neuropathic Pain-Related Behavior by Preventing MMP-9 Activation and, Consequently, Pronociceptive Interleukin Release in a Rat Model. Front Pharmacol 8**:** 48.

Lochner M, & Thompson AJ (2014). The antimalarial drug proguanil is an antagonist at 5-HT_3 receptors. J Pharmacol Exp Ther 351**:** 674-684.

Lochner M, & Thompson AJ (2015). A review of fluorescent ligands for studying 5-HT_3 receptors. Neuropharmacology 98**:** 31-40.

Logie L, Harthill J, Patel K, Bacon S, Hamilton DL, Macrae K*, et al.* (2012). Cellular responses to the metal-binding properties of metformin. Diabetes 61**:** 1423-1433.

Matsumura Y, Yamashita T, Sasaki A, Nakata E, Kohno K, Masuda T*, et al.* (2016). A novel P2X4 receptor-selective antagonist produces anti-allodynic effect in a mouse model of herpetic pain. Sci Rep 6**:** 32461.

Muller CE (2015). Medicinal chemistry of P2X receptors: allosteric modulators. Curr Med Chem 22**:** 929-941.

North RA, & Jarvis MF (2013). P2X receptors as drug targets. Mol Pharmacol 83**:** 759-769.

Oury C, Kuijpers MJ, Toth-Zsamboki E, Bonnefoy A, Danloy S, Vreys I*, et al.* (2003). Overexpression of the platelet P2X1 ion channel in transgenic mice generates a novel prothrombotic phenotype. Blood 101**:** 3969-3976.

Pan CC, Kuo DH, Shieh P, Chen FA, Kuo CC, & Jan CR (2010). Effect of the Antidepressant Paroxetine on Ca2+ Movement in PC3 Human Prostate Cancer Cells. Drug Develop Res 71**:** 120-126.

Ralevic V (2015). P2X Receptors in the Cardiovascular System and their Potential as Therapeutic Targets in Disease. Current Medicinal Chemistry 22: 851-865.

Ruepp MD, Brozik JA, de Esch IJ, Farndale RW, Murrell-Lagnado RD, & Thompson AJ (2015). A fluorescent approach for identifying P2X1 ligands. Neuropharmacology 98**:** 13-21.

Syed NiH, & Kennedy C (2012). Pharmacology of P2X receptors. Wiley Interdisciplinary Reviews: Membrane Transport and Signaling 1**:** 16-30.

Thompson AJ, Verheij MH, Leurs R, De Esch IJ, & Lummis SC (2010). An efficient and information-rich biochemical method design for fragment library screening on ion channels. Biotechniques 49**:** 822-829.

Thompson AJ, Verheij MH, van Muijlwijk-Koezen JE, Lummis SC, Leurs R, & de Esch IJ (2013). Structure-activity relationships of quinoxaline-based 5-HT_3A and 5-HT_3AB receptor-selective ligands. ChemMedChem 8**:** 946-955.

Tsuda M, Kuboyama K, Inoue T, Nagata K, Tozaki-Saitoh H, & Inoue K (2009). Behavioral phenotypes of mice lacking purinergic P2X4 receptors in acute and chronic pain assays. Mol Pain 5**:** 28.

Tsuda M, Masuda T, Tozaki-Saitoh H, & Inoue K (2013). P2X4 receptors and neuropathic pain. Front Cell Neurosci 7**:** 191.

Ushioda M, Kobayashi K, Saito D, Sakuma S, Imai T, & Inoue K Preparation of benzodiazepine derivatives P2X4 receptor antagonists WO 2013105608 A1.

Verheij MH, Thompson AJ, van Muijlwijk-Koezen JE, Lummis SC, Leurs R, & de Esch IJ (2012). Design, synthesis, and structure-activity relationships of highly potent 5-HT_3 receptor ligands. J Med Chem 55**:** 8603-8614.

von Borstel Smith M, Crofoot K, Rodriguez-Proteau R, & Filtz TM (2007). Effects of phenytoin and carbamazepine on calcium transport in Caco-2 cells. Toxicol In Vitro 21**:** 855-862.

White CW, Choong YT, Short JL, Exintaris B, Malone DT, Allen AM*, et al.* (2013). Male contraception via simultaneous knockout of α1A-adrenoceptors and P2X1-purinoceptors in mice. Proc Natl Acad Sci U S A 110**:** 20825-20830.

Zabala A, Vazquez-Villoldo N, Rissiek B, Gejo J, Martin A, Palomino A*, et al.* (2018). P2X4 receptor controls microglia activation and favors remyelination in autoimmune encephalitis. EMBO Mol Med 10, e8743

Figure Legends

Fig 1. Compounds reported to have activity at P2X4 receptors.

Fig 2. Flow chart of compound survival (number of compounds in brackets) during each stage of the *in silico* screen.

Fig 3. ATP bound to the P2X4 co-crystal structure (4DW1), and examples of two docked poses (**57** and **66)**. Upper panels show cartoon representations of each pose, and the lower panels are ligand interaction diagrams. The circle highlights the binding site that is shown in panels B and C. (A) In 4DW1 the purine interacts with the backbones of K67 and T186, and the α, β and γ phosphates with S289, K313 and R295 respectively. (B) For **57** the ether oxygen interacts with K69 and the amine with the backbone of L214. The two aromatic rings are flanked by the sidechains of K67, K69, L188, I223, and I229. (C) The imidazole in **66** undergoes π-stacking with H140, the alcohol is stabilised by a backbone interaction with K215, and the aromatic ring is located in a hydrophobic groove created by K67, K69, L188 and I229.

Fig 4. Effects of selected fragments on hP2X4, measured using TEVC. (A-D) Concentration-dependent effects of selected fragments on the 3 μM ATP response. (E) Effects of the same fragments on uninjected oocytes, showing that 300 μM **38**, **57** and **66** have no measureable effects, while 300 μM **35** causes a hyperpolarising response. (F) The hyperpolarising effect of 30 μM **35** was evident immediately before the depolarising current evoked by ATP (note the small upward deflection of the trace) and is likely to be responsible for the apparent reduction in the amplitude of the depolarising ATP response. This summation of the two effects could be mistaken for hP2X4 receptor inhibition.

Fig 5. Concentration-dependent inhibition of the hP2X1 response measured using TEVC. Example concentration-response relationships are shown for **196** (A) and **216** (B). Parameters derived from these curves can be found in Table 4. *Inset* is an example trace showing the hP2X1 response to 0.5 μM ATP (EC_{50}: black horizontal bar).

Fig 6. Inhibition of hP2X4 by UoS14919. (A) UoS14919 inhibition of the hP2X4 response observed by FMA. (B) UoS14919 inhibition of the hP2X4 response observed by TEVC. Black line = 3 μM ATP, grey line = 10 μM UoS14919. (C) Using TEVC, no inhibition of the hP2X4 response was seen in the

presence of 75 µM PSB-12054 or 93 µM acridinol (maximal concentration, limited by solubility), and was consistent with a similar lack of inhibition using FMA. In this panel, the response to 3 µM ATP alone is shown in black (1) and the co-application of 3 µM ATP + compound is shown in grey (2). Applications of (1) and (2) are 3 min apart, but have been overlaid to show the similarity in the response.

Fig 1

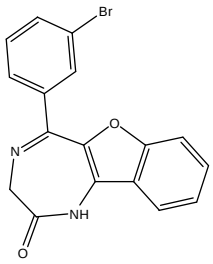

5-BDBD

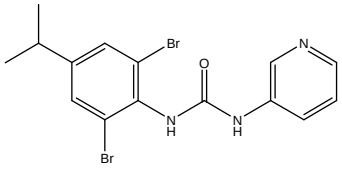

BX 430

Ivermectin

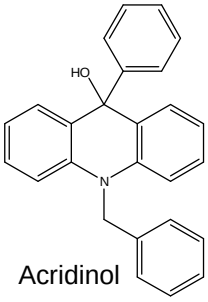

Acridinol

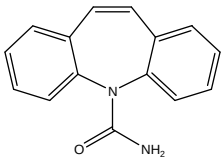

Carbamazepine

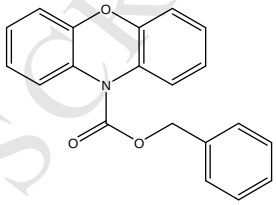

Pheonoxazine
PSB-12054

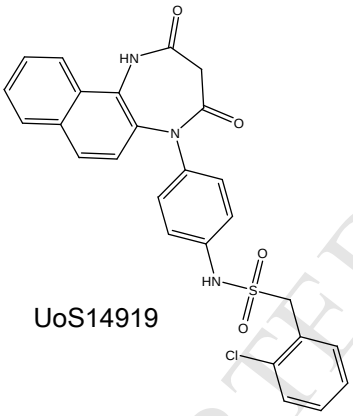

UoS14919

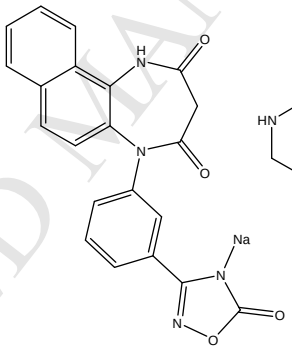

NP-1815 _PX

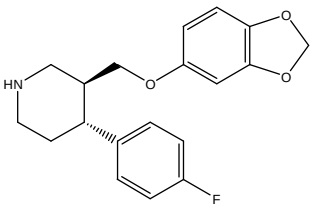

Paroxetine

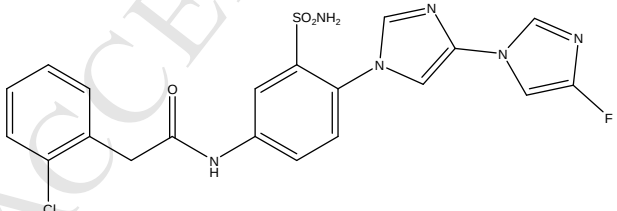

Bayer (WO 2018210729A1)

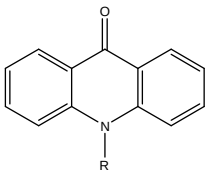

9 (10*H*) -acridanone

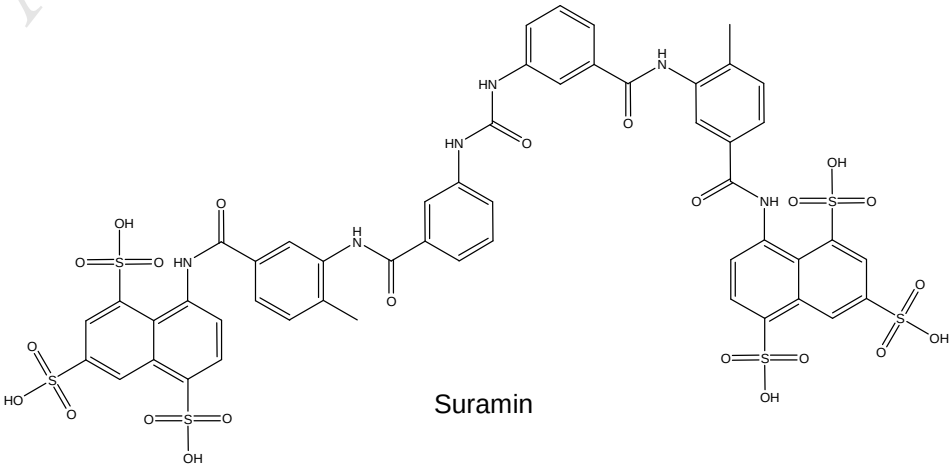

Suramin

Fig 2

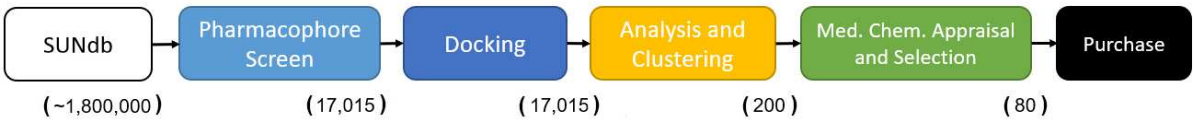

Fig 3

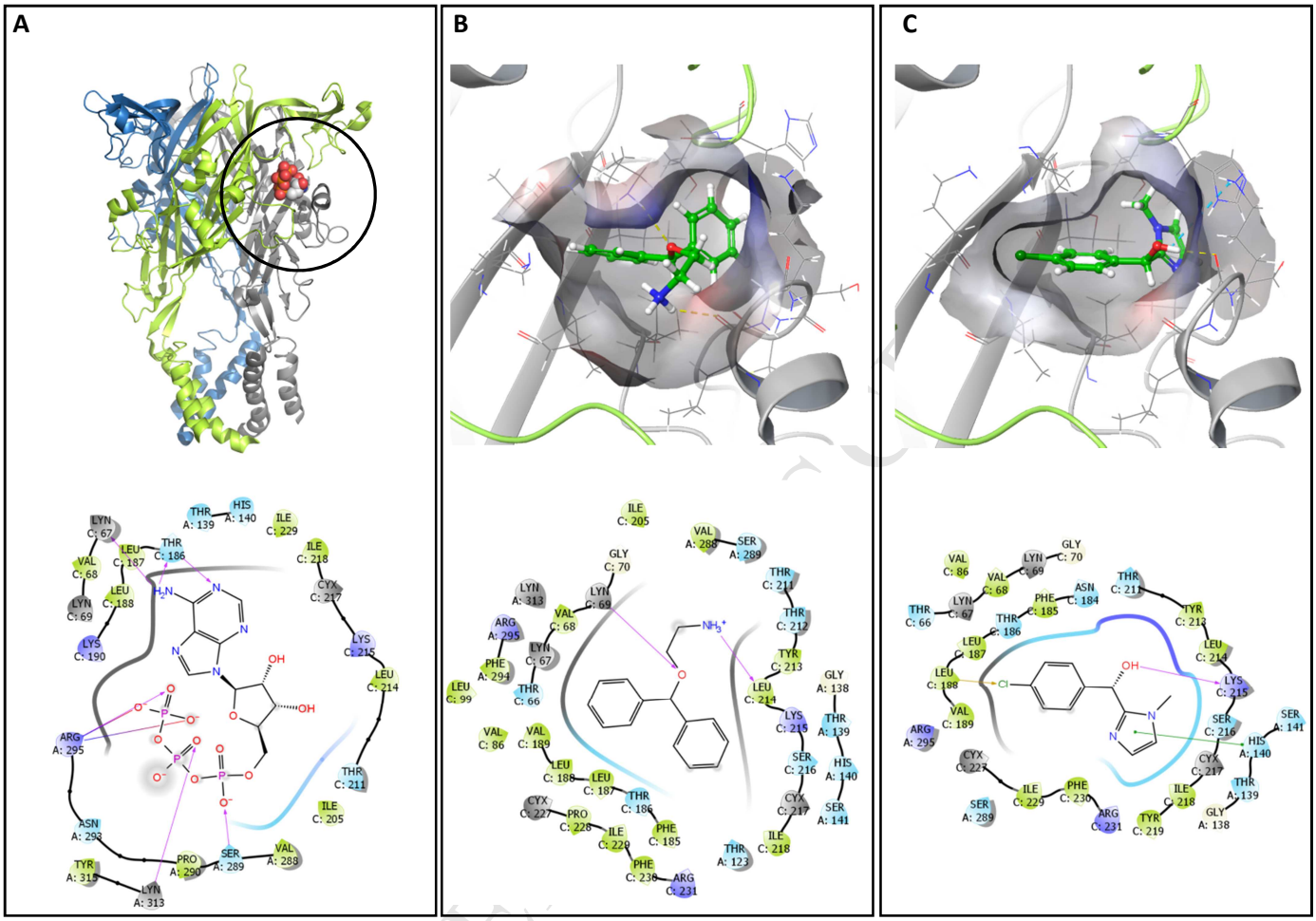

Fig 4

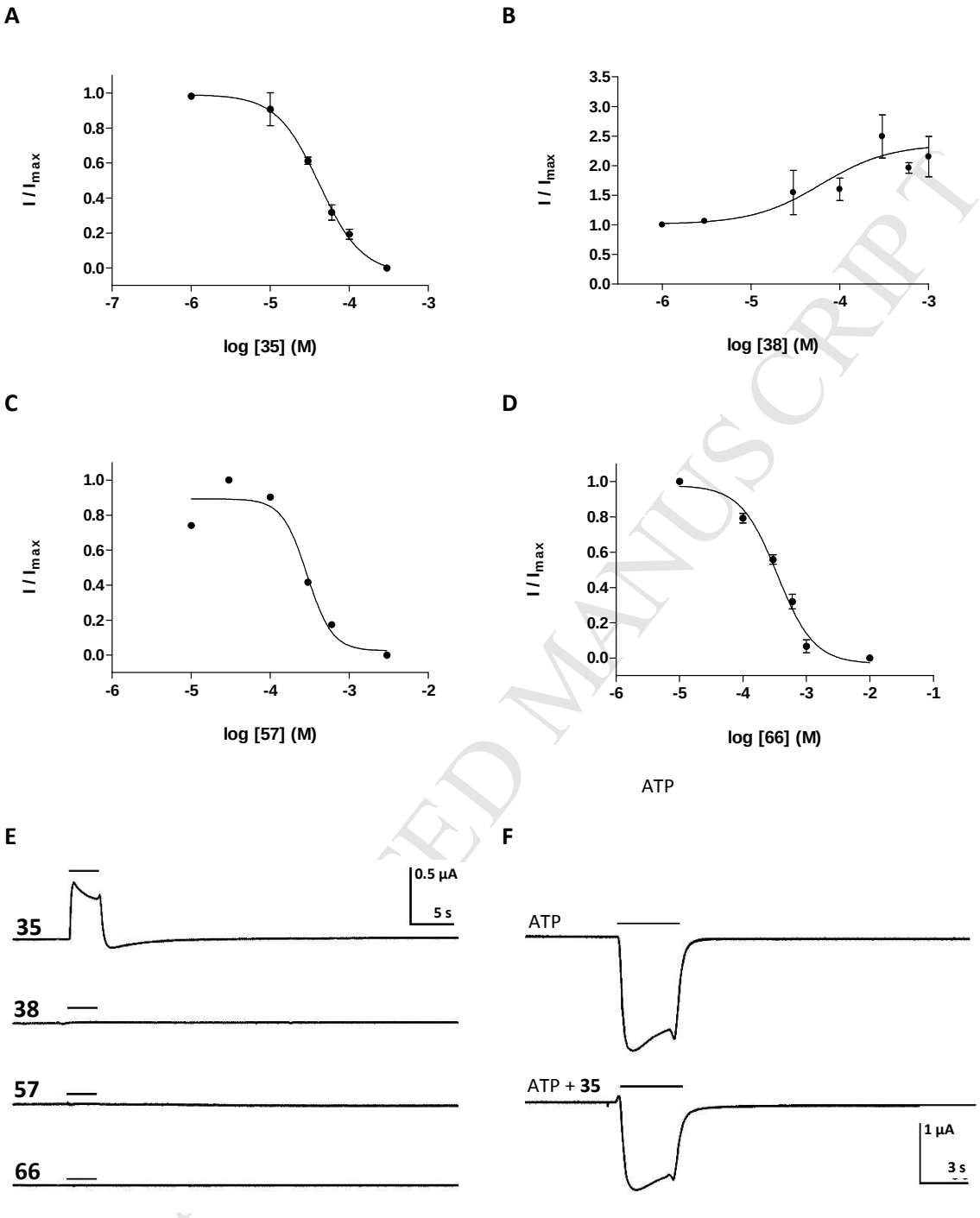

[Fragment]	*pIC_{50}*	*IC_{50} (µM)*	*n_H*	*n*
35	4.38 ± 0.05	42	1.6	3
57	3.53 ± 0.12	295	2.7	3
66	3.46 ± 0.05	347	1.5	4

Fig 5

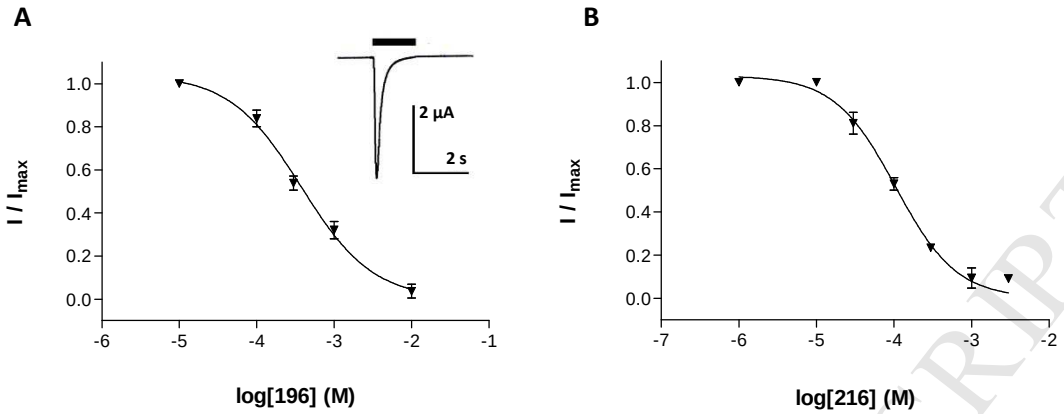

Fig 6

A

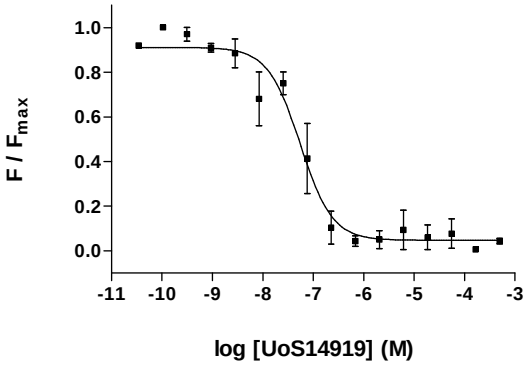
1.0
0.8
0.6
0.4
0.2
0.0
F / Fmax
-11
-10
-9
-8
-7
-6
-5
-4
-3
log [UoS14919] (M)

B

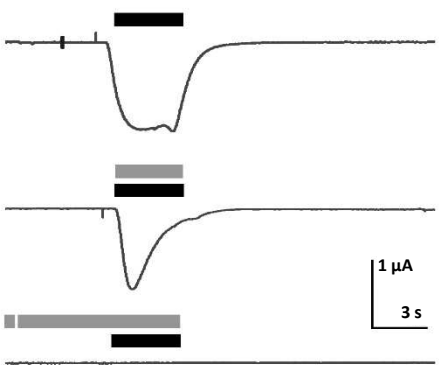
1 µA
3 s

C

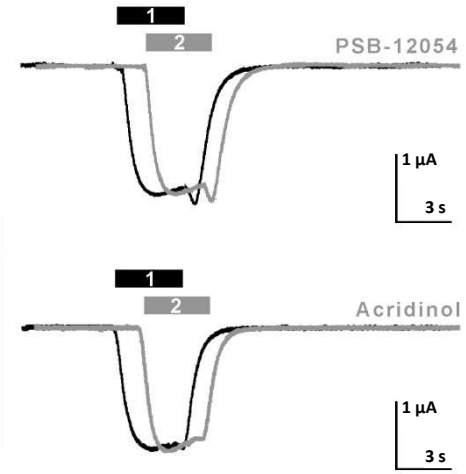
1
2
PSB-12054
1 µA
3 s
1
2
Acridinol
1 µA
3 s

Table 1: Single point FMA screening on hP2X4 stably expressed in HEK293T cells. Test fragments were identified from an *in silico* screen of an hP2X4 homology model that was based on the zebrafish P2X4-ATP co-crystal structure (4DW1).

	hP2X4		**hP2X1**		
Compound	**F / Fmax**	***n***	**F / Fmax**	***n***	**Structure**
1	0.50 ± 0.19	3	0.63 ± 0.07	4	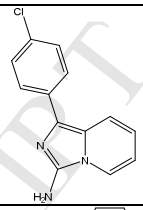
2	0.36 ± 0.01	3	0.51 ± 0.04	4	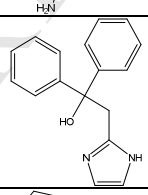
3	0.53 ± 0.02	3	0.31 ± 0.05	3	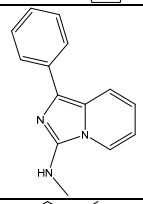
4	0.75 ± 0.08	3	0.57 ± 0.06	4	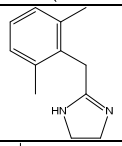
5	0.77 ± 0.09	3	0.27 ± 0.07	3	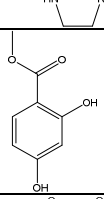
6	0.64 ± 0.09	3	0.44 ± 0.11	4	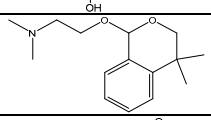
7	0.61 ± 0.07	3	0.29 ± 0.10	3	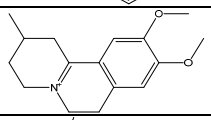
8	0.67 ± 0.16	3	0.46 ± 0.09	4	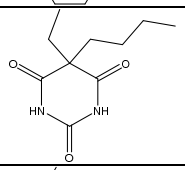
9	0.65 ± 0.08	3	0.38 ± 0.09	4	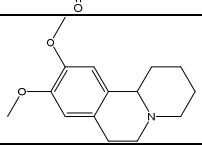
10	0.39 ± 0.03	3	0.43 ± 0.1	4	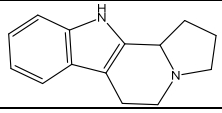

11	0.80 ± 0.08	3	0.36 ± 0.08	4	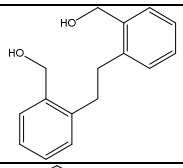
12	0.47 ± 0.09	3	0.08 ± 0.09	3	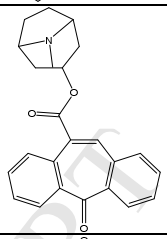
13	1.06 ± 0.08	3	0.43 ± 0.11	4	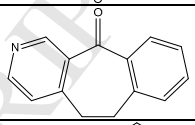
14	0.42 ± 0.09	3	0.27 ± 0.08	4	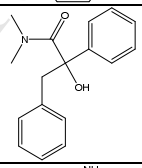
15	0.78 ± 0.05	3	0.36 ± 0.11	4	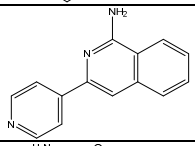
16	0.77 ± 0.13	3	0.36 ± 0.08	4	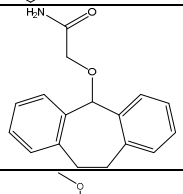
17	0.70 ± 0.05	3	0.35 ± 0.06	3	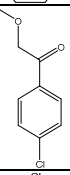
18	0.49 ± 0.19	3	0.35 ± 0.09	4	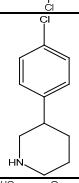
19	0.71 ± 0.13	3	0.33 ± 0.03	4	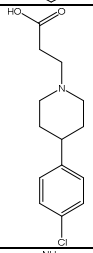
20	0.12 ± 0.05	3	0.10 ± 0.04	4	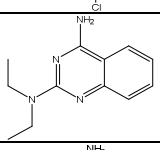
21	0.35 ± 0.11	3	0.12 ± 0.03	4	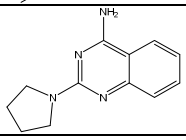

22	0.44 ± 0.09	3	0.26 ± 0.08	3	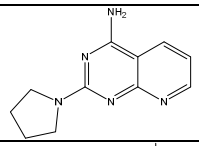
23	0.41 ± 0.08	3	0.45 ± 0.11	3	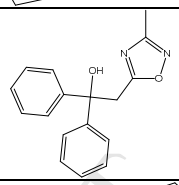
24	0.49 ± 0.14	3	0.53 ± 0.08	3	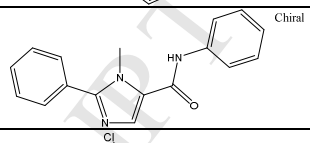
25	0.58 ± 0.06	3	0.53 ± 0.07	3	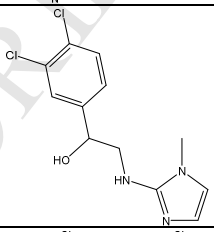
26	0.66 ± 0.07	3	0.51 ± 0.06	3	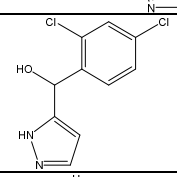
27	0.77 ± 0.04	3	0.47 ± 0.05	3	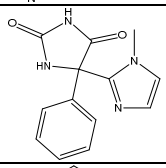
28	0.77 ± 0.05	3	0.44 ± 0.06	3	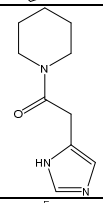
29	0.83 ± 0.08	3	0.58 ± 0.03	3	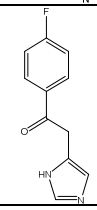
30	0.44 ± 0.07	3	0.60 ± 0.11	3	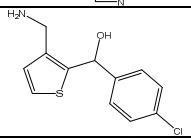
31	0.66 ± 0.07	3	0.46 ± 0.03	3	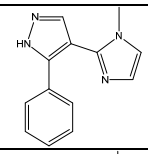
32	0.29 ± 0.14	3	0.52 ± 0.06	3	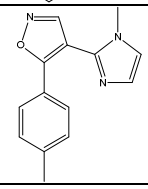

33	0.64 ± 0.21	3	0.41 ± 0.04	3	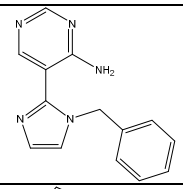
34	0.35 ± 0.10	3	0.14 ± 0.03	3	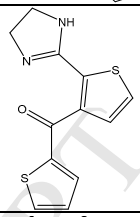
35	0.05 ± 0.02	3	0.28 ± 0.12	3	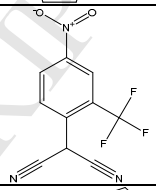
36	0.81 ± 0.13	3	0.48 ± 0.04	3	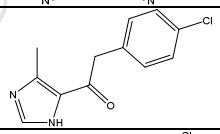
37	0.58 ± 0.05	3	0.56 ± 0.11	3	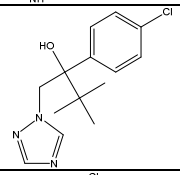
38	0.31 ± 0.28	3	0.22 ± 0.10	3	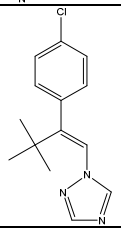
39	0.68 ± 0.01	3	0.24 ± 0.16	3	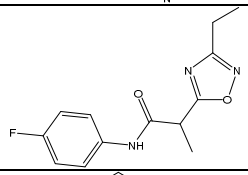
40	0.64 ± 0.05	3	0.69 ± 0.30	3	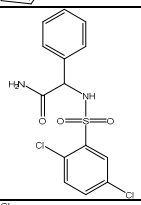
41	0.82 ± 0.04	3	0.62 ± 0.09	3	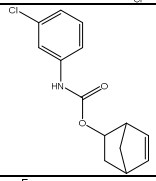
42	0.76 ± 0.06	3	0.65 ± 0.10	3	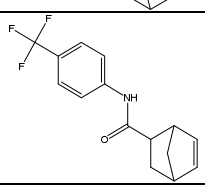

43	0.76 ± 0.08	3	0.46 ±0.07	3	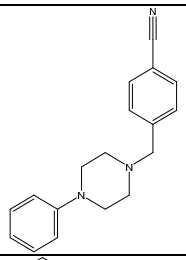
44	0.64 ± 0.09	3	0.47± 0.11	3	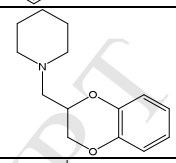
45	0.71 ± 0.06	3	0.56 ± 0.07	3	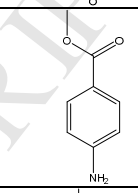
46	0.67 ± 0.02	3	0.32 ± 0.11	3	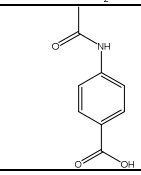
47	0.62 ± 0.05	3	0.64 ± 0.23	3	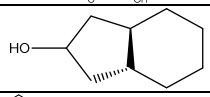
48	0.62 ± 0.07	3	0.45 ± 0.22	3	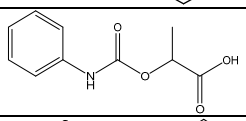
49	0.82 ± 0.09	3	0.56 ± 0.09	3	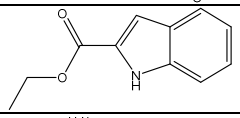
50	0.58 ± 0.11	3	0.74 ± 0.39	3	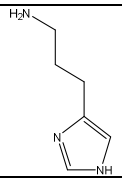
63	0.67 ± 0.12	3	0.60 ± 0.03	3	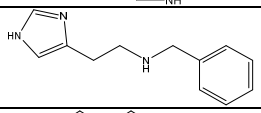
52	0.79 ± 0.06	3	0.46 ±0.05	3	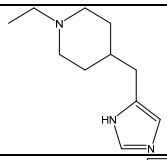
53	0.56 ± 0.09	3	0.29 ± 0.06	3	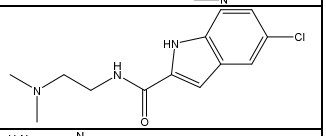
54	0.93 ± 0.08	3	0.68 ± 0.03	3	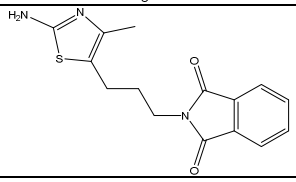

55	0.49 ± 0.05	3	0.80 ± 0.01	3	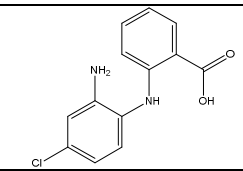
56	0.51 ± 0.06	3	0.30 ± 0.03	3	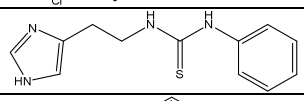
57	0.21 ± 0.21	3	0.57 ± 0.13	3	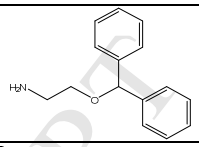
58	0.59 ± 0.11	3	0.50 ± 0.08	3	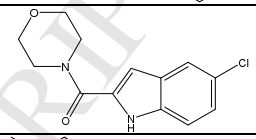
59	0.71 ± 0.15	3	0.41 ± 0.05	3	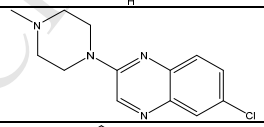
60	0.75 ± 0.03	3	0.61 ± 0.01	3	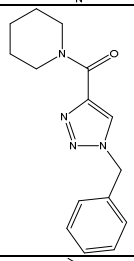
61	0.65 ± 0.09	3	0.67 ± 0.03	3	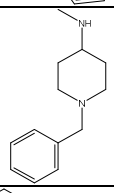
62	0.59 ± 0.06	3	0.82 ± 0.05	3	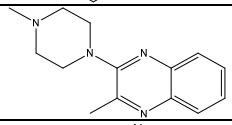
63	0.61 ± 0.40	3	0.62 ± 0.02	3	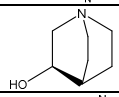
64	0.23 ± 0.19	3	0.72 ± 0.10	3	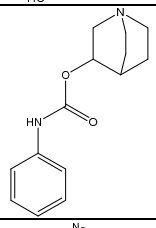
65	0.72 ± 0.12	3	0.69 ± 0.10	3	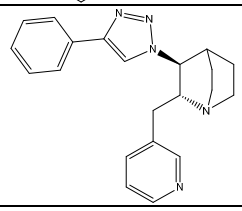

66	0.30 ± 0.11	3	0.65 ± 0.11	3	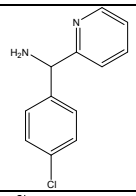
67	0.75 ± 0.08	3	0.46 ± 0.02	3	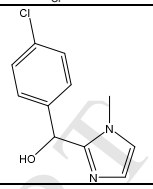
68	0.71 ± 0.06	3	0.69 ± 0.01	3	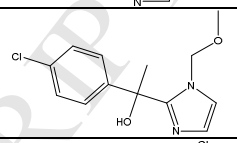
69	0.72 ± 0.07	3	0.67 ± 0.05	3	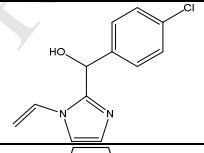
70	0.62 ± 0.09	3	0.64 ± 0.03	3	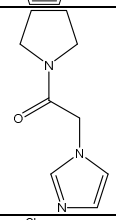
71	0.56 ± 0.09	3	0.70 ± 0.01	3	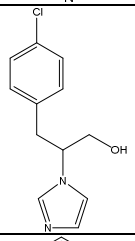
72	0.60 ± 0.10	3	-	-	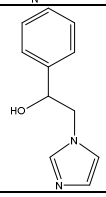
73	0.65 ± 0.10	3	0.39 ± 0.07	3	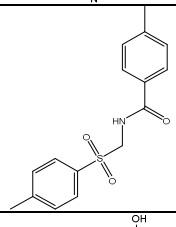
74	0.88 ± 0.08	3	-	-	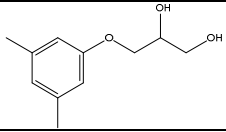
75	0.81 ± 0.07	3	-	-	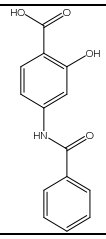

76	0.72 ± 0.10	3	-	-	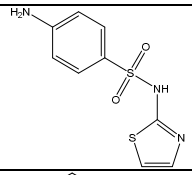
77	0.87 ± 0.06	3	-	-	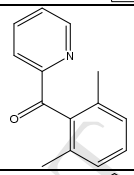
78	0.49 ± 0.08	3	-	-	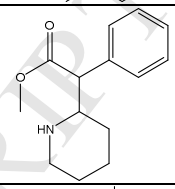
79	0.51 ± 0.09	3	-	-	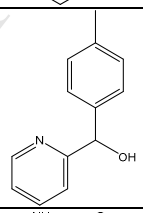
80	0.47 ± 0.09	3	-	-	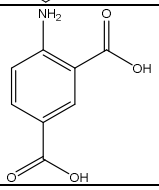

Fragments denoted with '-' were not tested on hP2X1 receptors owing to their limited availability.

Table 2: The top ten most potent hP2X4 ligands identified using single-point FMA screens, and subsequently validated with single-point TEVC assays.

	hP2X4				hP2X1			
Identifier	**FMA** **(F / F_{max})**	***n***	**TEVC** **(I / I_{max})**	***n***	**FMA** **(F / F_{max})**	***n***	**TEVC** **(I / I_{max})**	***n***
2	0.36 ± 0.01	3	1.19 ± 0.24	3	0.51 ± 0.04	4	1.10 ± 0.03	3
20	0.12 ± 0.05	3	0.95 ± 0.15	3	0.10 ± 0.04	4	0.72 ± 0.04	4
21	0.35 ± 0.11	3	0.95 ± 0.04	3	0.12 ± 0.03	4	0.52 ± 0.04	3
32	0.29 ± 0.14	3	1.15 ± 0.04	3	0.52 ± 0.06	3	0.57 ± 0.02	4
34	0.35 ± 0.10	3	0.78 ± 0.08	3	0.14 ± 0.03	3	0.08 ± 0.03	3
35*	0.05 ± 0.02	3	0.00 ± 0.00	3	0.28 ± 0.12	3	0.44 ± 0.02	4
38*	0.31 ± 0.28	3	2.49 ± 0.28	6	0.22 ± 0.10	3	1.01 ± 0.06	3
57*	0.21 ± 0.21	3	0.31 ± 0.10	3	0.57 ± 0.13	3	0.66 ± 0.01	4
64	0.23 ± 0.19	3	1.74 ± 0.24	3	0.72 ± 0.10	3	1.02 ± 0.04	3
66*	0.30 ± 0.11	3	0.31 ± 0.05	3	0.65 ± 0.11	3	0.95 ± 0.12	3

** These fragments yielded changes to the hP2X4-mediated response in both FMA and TEVC assays and were subjected to further testing (fig 3).*

Table 3A: Elaboration of initial hit fragments **20**, **21** and **22**, and assessment using single point TEVC assays on oocyte-expressed hP2X4.

Identifier	I / Imax	*n*	Structure
81	0.66 ± 0.06	4	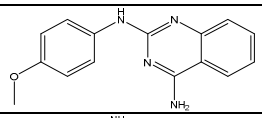
82	0.70 ± 0.08	3	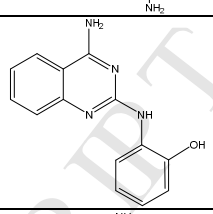
83	1.28 ± 0.05	4	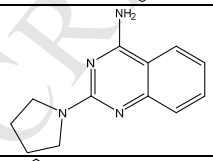
84	1.29 ± 0.23	3	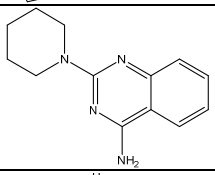
85	0.82 ±0.04	7	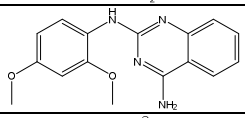
86	1.02 ± 0.10	3	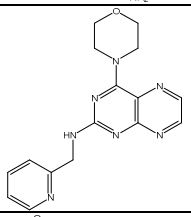
87	1.22 ± 0.13	4	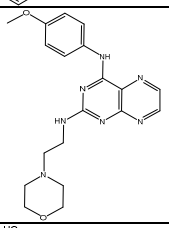
88	1.07 ± 0.10	6	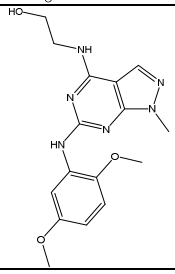

Table 3B: Further elaboration of initial hit fragments **20**, **21** and **22**, and assessment using single point TEVC assays on oocyte-expressed hP2X4.

Identifier	I / Imax	*n*	Structure
89	0.83 ± 0.06	7	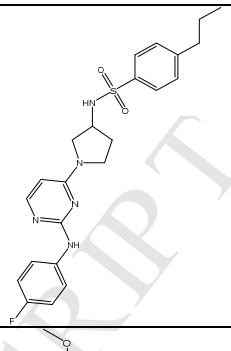
90	0.97 ± 0.01	3	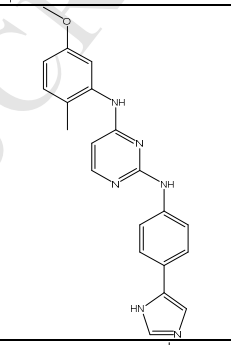
91	0.95 ± 0.10	3	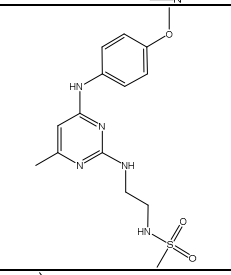
92	1.20 ± 0.08	5	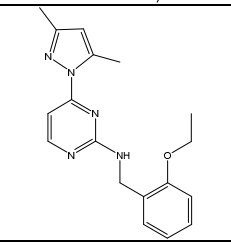

Table 3C: Elaboration of initial hit fragments **30**, **32** and **66**, and assessment using single point TEVC assays on oocyte-expressed hP2X4.

Identifier	I / Imax	*n*	Structure
93	1.42 ± 0.07	3	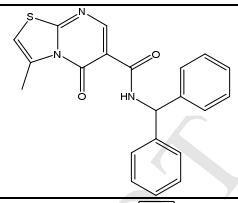
94	1.03 ± 0.04	4	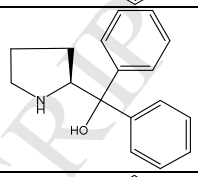
95	1.10 ± 0.03	3	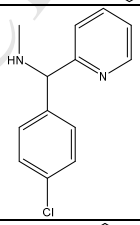
96	1.04 ± 0.07	3	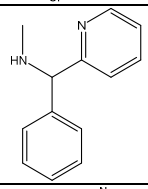
97	1.01 ± 0.01	3	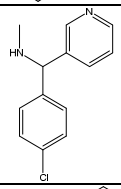
98	1.04 ± 0.12	3	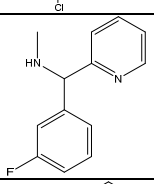
99	1.01 ± 0.26	3	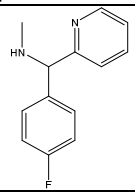
100	1.02 ± 0.11	3	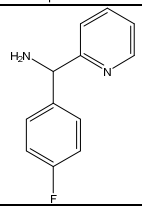

101	0.97 ± 0.03	3	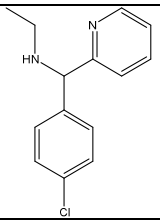
102	1.03 ± 0.13	4	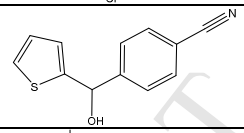
103	1.01 ± 0.11	3	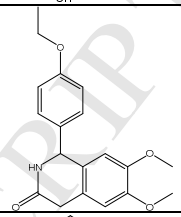
104	0.95 ± 0.01	3	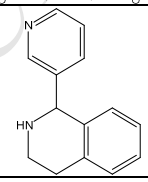
105	1.24 ± 0.08	3	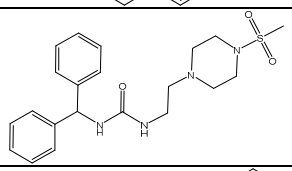
106	1.41 ± 0.04	3	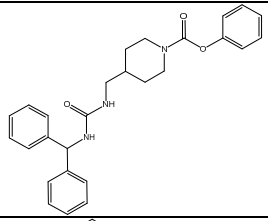
107	1.02 ± 0.09	4	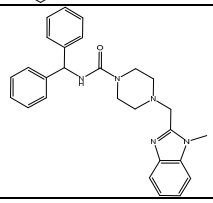

Table 3D: Elaboration of initial hit fragment **10**, and assessment using single point TEVC assays on oocyte-expressed hP2X4.

Identifier	I / Imax	*n*	Structure
108	0.90 ± 0.10	3	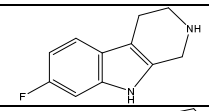
109	1.21 ± 0.17	4	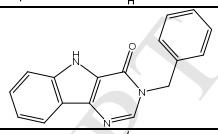
110	0.59 ± 0.11	4	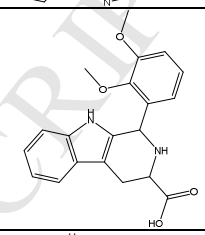
111	1.23 ± 0.08	5	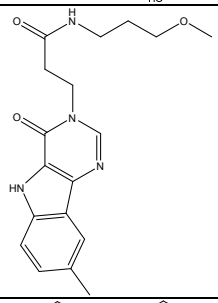
112	1.01 ± 0.10	4	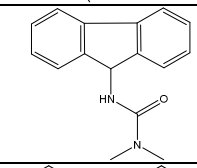
113	0.99 ± 0.11	3	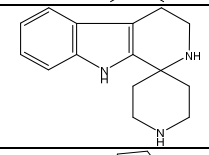
114	1.06 ± 0.07	3	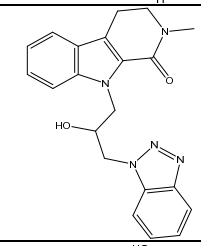
115	1.07 ± 0.03	4	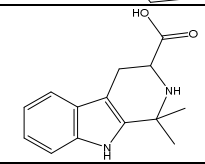
116	1.19 ± 0.05	3	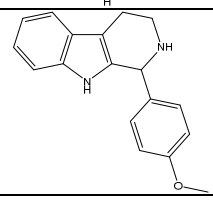

117	0.93 ± 0.02	3	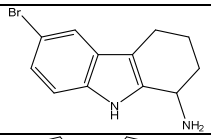
118	1.08 ± 0.30	3	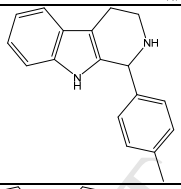
119	0.82 ± 0.05	3	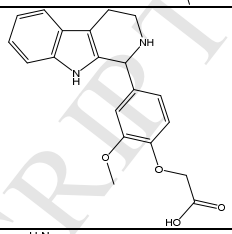
120	0.98 ± 0.14	3	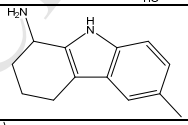
121	0.88 ± 0.07	3	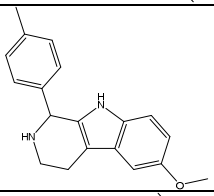
122	0.77 ± 0.13	3	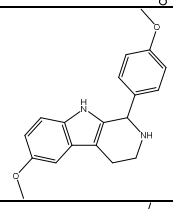
123	0.89 ± 0.06	5	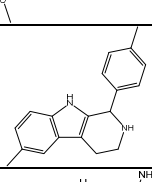
124	0.76 ± 0.05	5	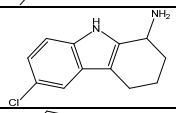
125	1.38 ± 0.13	4	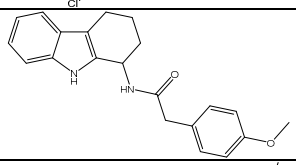
126	1.43 ± 0.10	5	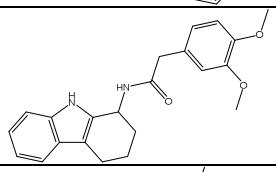
127	0.80 ± 0.06	4	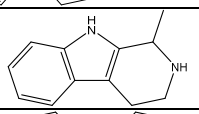
128	0.93 ± 0.09	2	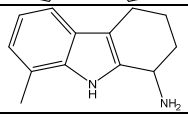

129	0.74 ± 0.01	3	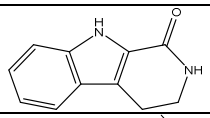
130	0.65 ± 0.05	3	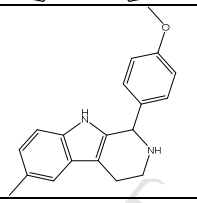
131	1.05 ± 0.13	3	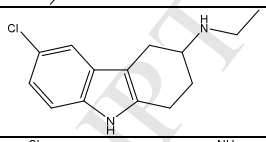
132	1.10 ± 0.10	3	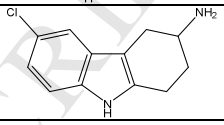
133	0.53 ± 0.03	3	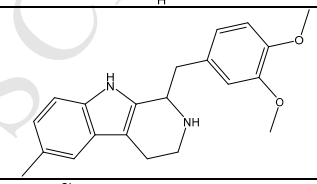
134	0.79 ± 0.02	3	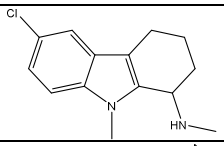
135	0.98 ± 0.08	3	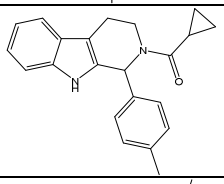
136	0.77 ± 0.07	3	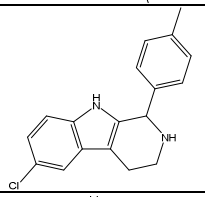
137	0.72 ± 0.05	3	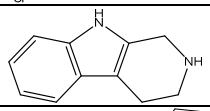
138	1.09 ± 0.13	3	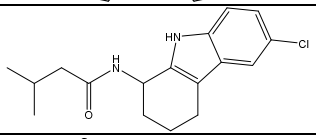
139	0.86 ± 0.09	3	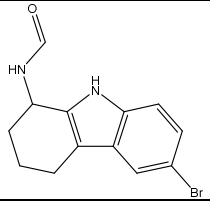
140	0.84 ± 0.12	3	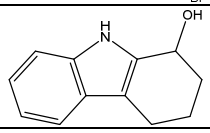

141	0.87 ± 0.08	3	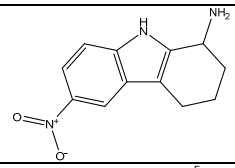
142	0.41 ± 0.05	3	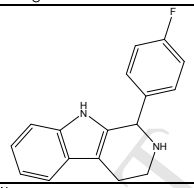
143	1.04 ± 0.05	3	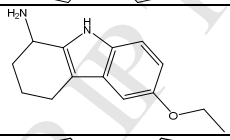
144	0.89 ± 0.03	3	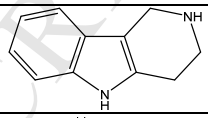
145	1.07 ± 0.01	3	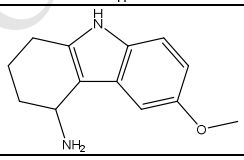

Table 3E: Probing the indole substructure of initial hit fragment **10** by single point TEVC assays on oocyte-expressed hP2X4.

Identifier	I / Imax	*n*	Structure
146	0.67 ± 0.03	4	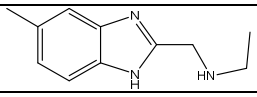
147	1.16 ± 0.09	5	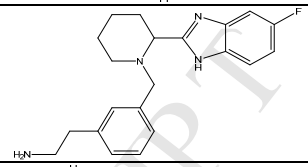
148	1.19 ± 0.10	4	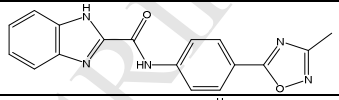
149	0.52 ± 0.05	4	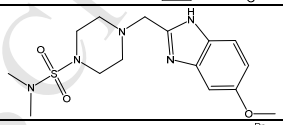
150	0.65 ± 0.12	4	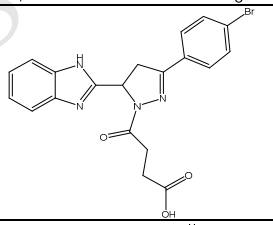
151	0.66 ± 0.05	5	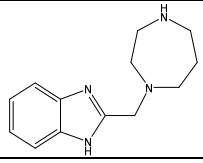
152	0.84 ± 0.05	5	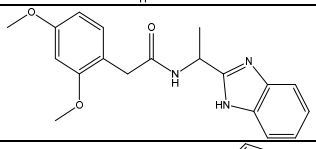
153	0.88 ± 0.13	2	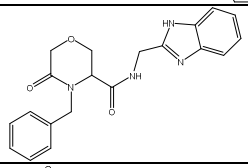
154	0.78 ± 0.07	6	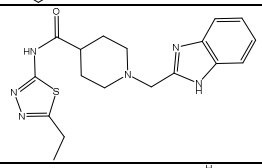
155	1.01 ± 0.06	3	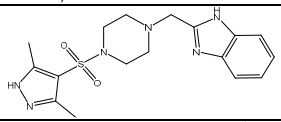
156	1.05 ± 0.09	3	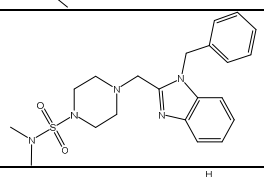
157	0.97 ± 0.04	3	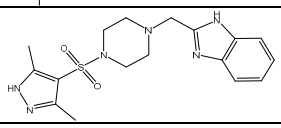

158	0.92 ± 0.06	3	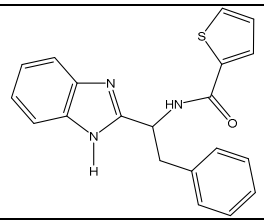
159	0.8 ± 0.05	6	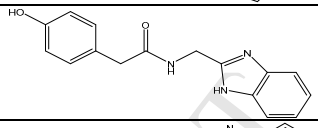
160	1.05 ± 0.06	3	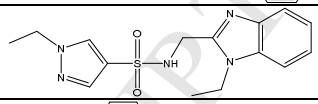
161	1.03 ± 0.20	3	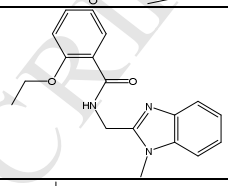
162	1.17 ± 0.31	3	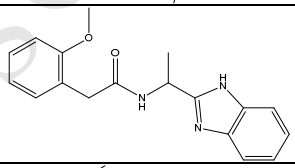
163	0.85 ± 0.02	3	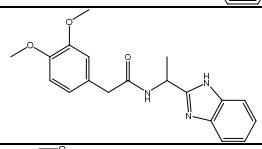
164	1.12 ± 0.16	4	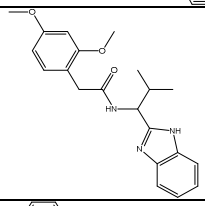
165	1.40 ± 0.13	6	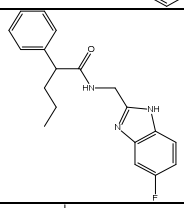
166	1.23 ± 0.13	3	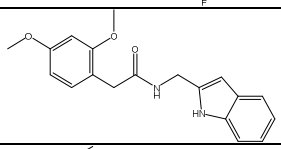
167	1.09 ± 0.16	6	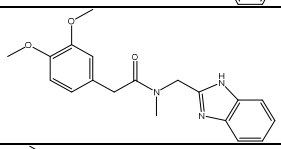
168	1.24 ± 0.25	5	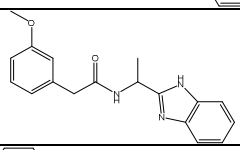
169	0.63 ± 0.04	5	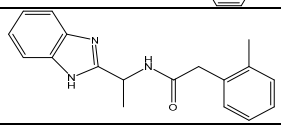

170	0.97 ± 0.05	3	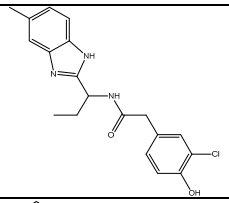
171	0.94 ± 0.10	3	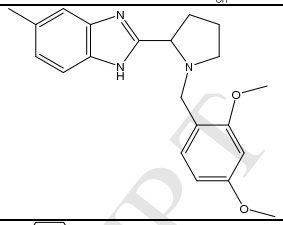
172	0.93 ± 0.02	3	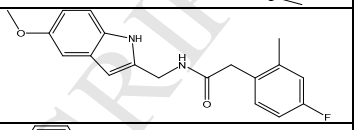
173	0.75 ± 0.04	3	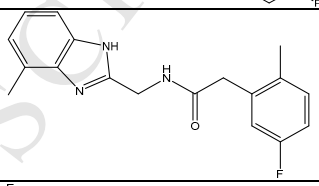
174	1.00 ± 0.04	3	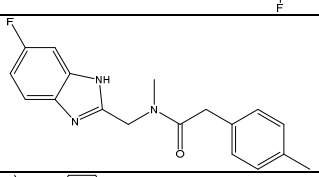
175	0.94 ± 0.04	3	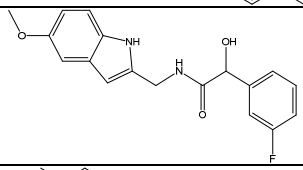
176	1.18 ± 0.19	3	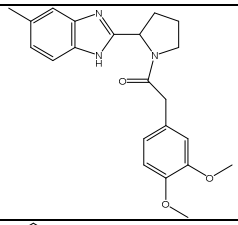
177	1.26 ± 0.09	3	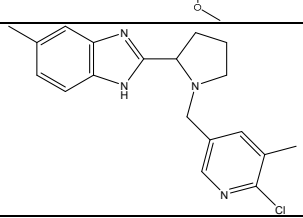
178	1.23 ± 0.02	3	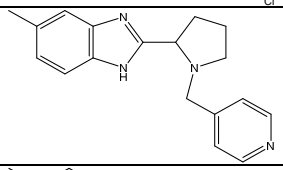
179	1.38 ± 0.17	3	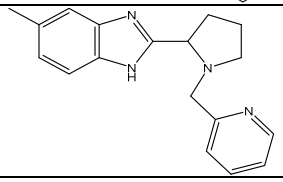

180	0.96 ± 0.06	3	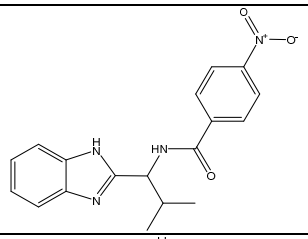
181	0.84 ± 0.16	3	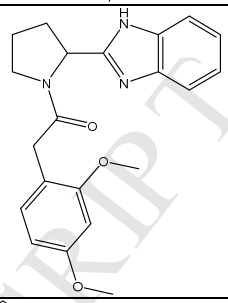
182	0.94 ± 0.07	3	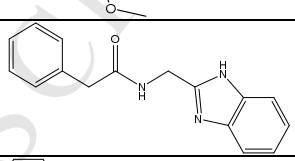
183	0.85 ± 0.010	3	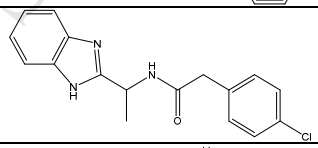
184	0.97 ± 0.02	3	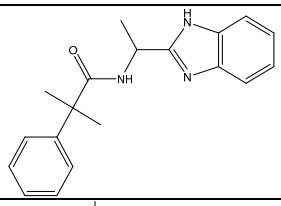
185	0.74 ± 0.03	3	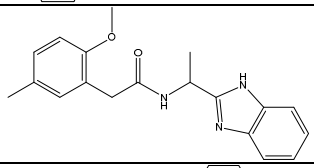
186	0.92 ± 0.03	3	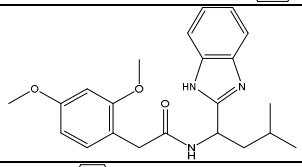
187	0.86 ± 0.06	3	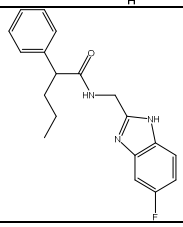
188	0.90 ± 0.05	3	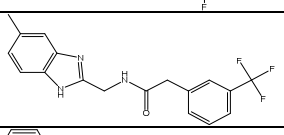
189	1.02 ± 0.12	3	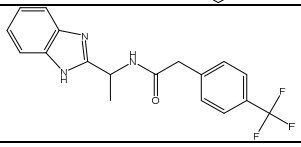

190	0.68 ± 0.05	3	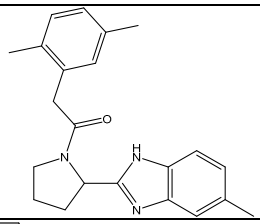
191	0.80 ± 0.01	3	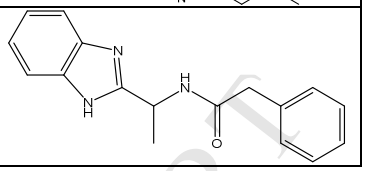

Table 4: Concentration-dependent actions of compounds tested using TEVC on oocyte-expressed hP2X1.

Compound	pIC_{50}	IC_{50} (mM)	*n*	Structure
192 (Proguanil)	2.95 ± 0.05	1.1	5	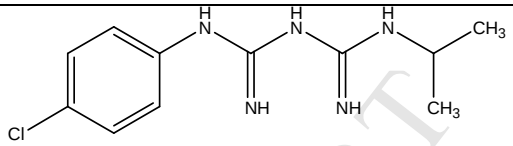
193 (*m*CPBG)	2.93 ± 0.05	1.2	5	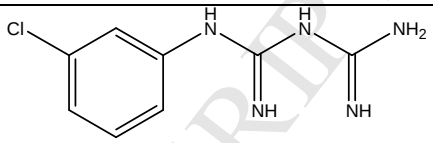
194	3.22 ± 0.06	1.1	5	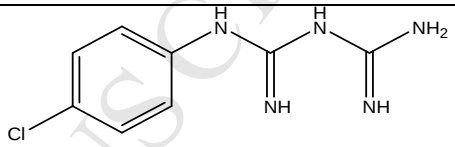
195	2.40 ± 0.03	4.0	4	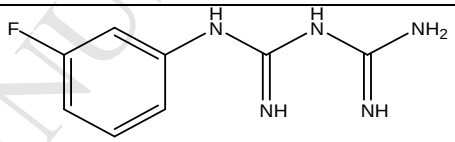
196	3.42 ± 0.06	0.38	5	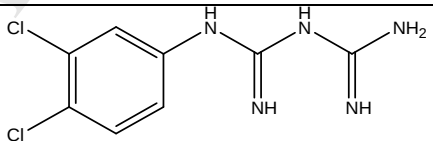
197	2.70 ± 0.08	2.0	5	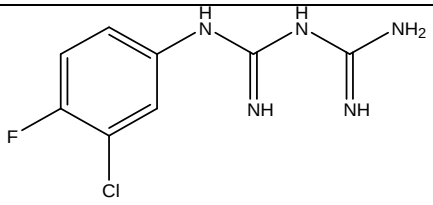
198	3.37 ± 0.06	0.42	3	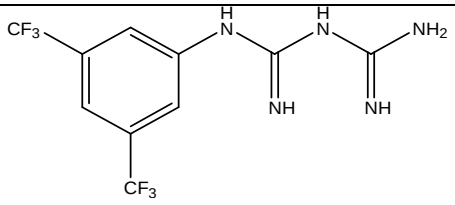
199	NE	-	3	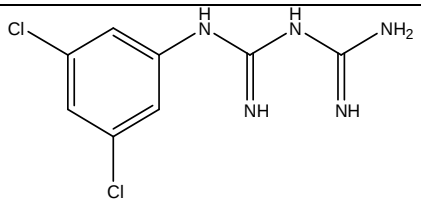
200	1.81 ± 0.01	15.4	3	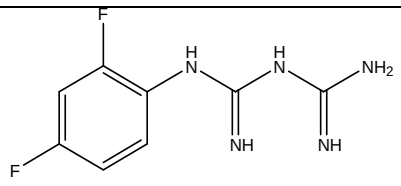

201	2.57 ± 0.20	2.7	3	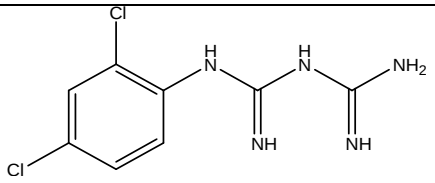
202	1.93 ± 0.15	11.7	3	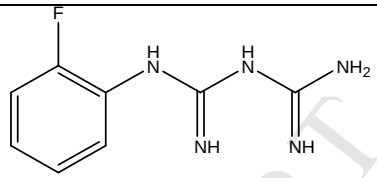
203	NE	-	3	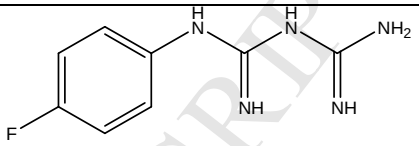
204	NE	-	4	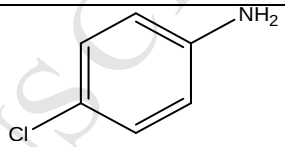
205	NE	-	3	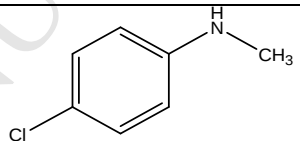
206	3.50 ± 0.04	0.32	7	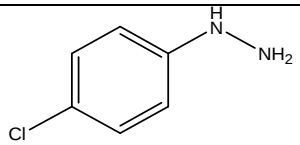
207	3.20 ±0.03	0.63	3	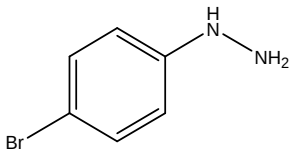
208 (Metformin)	NE	-	3	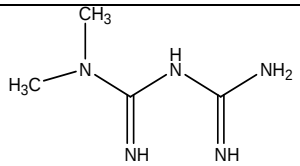
209	NE	-	7	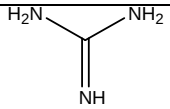
210	2.39 ±0.03	4.1	5	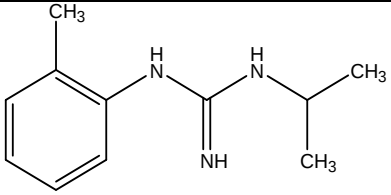
211	NE	-	3	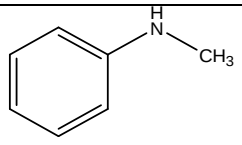

212	NE	-		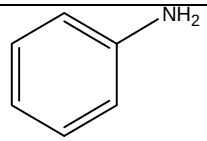
213	NE	-	3	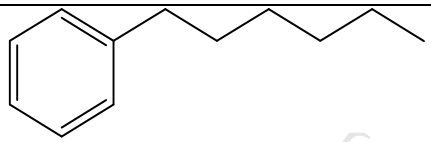
214	NE	-	3	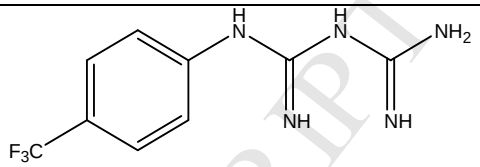
215	NE	-	3	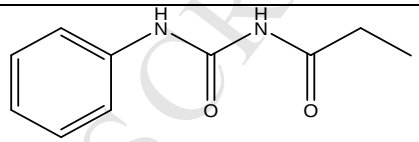
216	3.98 ± 0.05	0.10	3	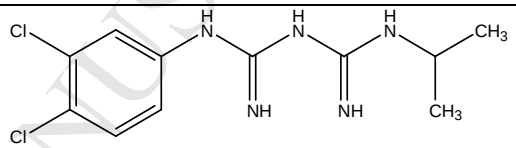
217	NE	-	3	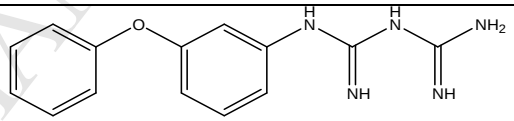
218	2.92 ± 0.11	1.2	5	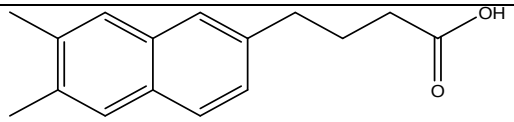
219	1.09 ± 0.09	81.3	3	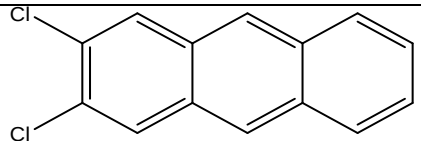
220	NE	-	3	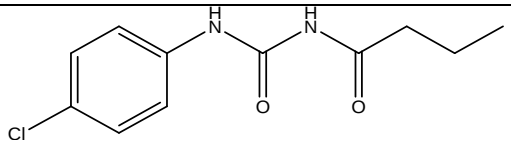
221	2.73 ± 0.06	1.9	3	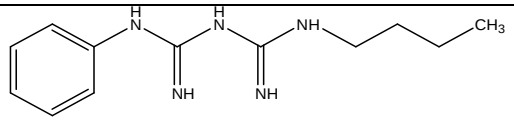
222	3.49 ± 0.04	0.32	3	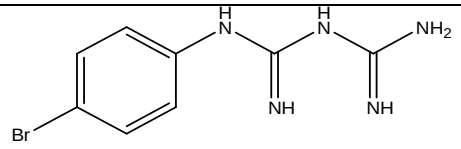

223	2.95 ± 0.05	1.1	3	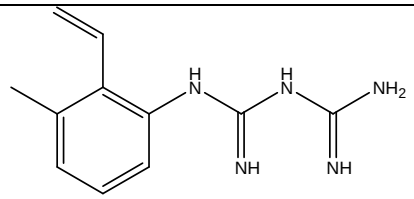
224	NE	-	3	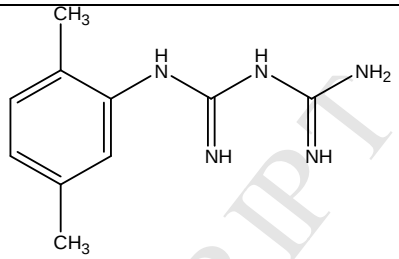
225	3.42 ± 0.04	0.38	3	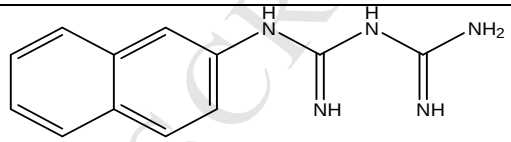
226	2.36 ±0.04	4.3	3	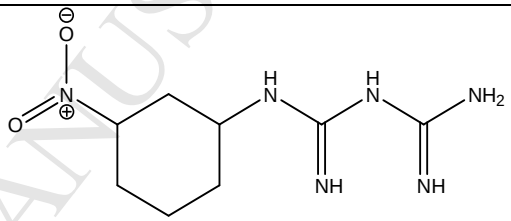
227	3.40 ± 0.08	0.40	3	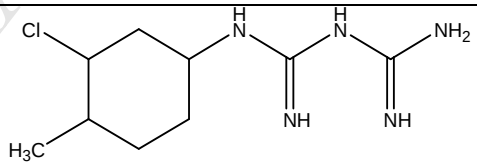

Highlights:

- We aimed to identify novel P2X1 and P2X4 receptor ligands
- We used a combination if in silico screening, fluorescence and two-electrode voltage clamp
- Only minor improvements in potency were achieved
- We highlight the challenge of identifying compounds that target this receptor class
- We suggest that at least two complimentary approaches are needed to confirm novel hits